

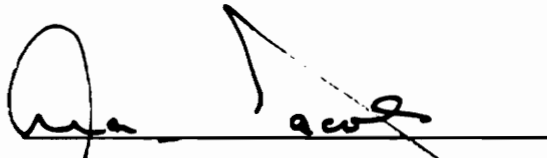
**Analysis and modeling of the effects of reflection induced noise on the
performance of fiber optic communication systems**

by

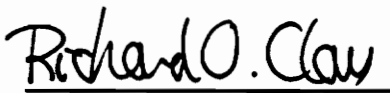
Ashok S. Raman

Thesis submitted to the Faculty of the
Virginia Polytechnic Institute and State University
in partial fulfillment of the requirements for the degree of
Masters of Science
in
Electrical Engineering

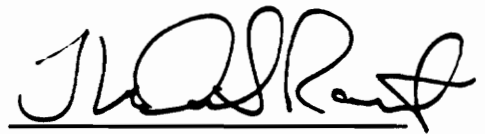
APPROVED:



Dr. Ira Jacobs, Chairman



Dr. R.O. Claus



Dr. T.S. Rappaport

July , 1990
Blacksburg, Virginia

c2

LD
5655
V855
1990
R353
c.2

Analysis and modeling of the effects of reflection induced noise on the performance of fiber optic communication systems

by
Ashok S. Raman

Dr. Ira Jacobs, Chairman
Electrical Engineering

(ABSTRACT)

Refractive index discontinuities in fiber optic transmission systems are known to cause deleterious effects. Non-negligible return losses associated with connectors and splices in present day systems cause intermittent error bursts and bit-error-rate floors in gigabit per second systems. These are attributed to the interferometric conversion of laser phase noise into signal-dependent intensity noise. This relative intensity noise (RIN) is substantially higher than the intrinsic RIN of the laser. The power spectral density of the RIN and its impact on the performance of incoherent on-off keying digital systems are calculated.

The combined effects of this noise and other degradations present in the system are studied using a simple model. It is shown that even though RIN is a bounded degradation, it, particularly in conjunction with other impairments, results in high and sometimes unacceptable power penalties. Previous analyses are extended to include the effects of multiple reflections from a single pair of reflectors, the effects of a multiplicity of reflection points and the combined effects of reflection-induced noise and other impairments. It is shown that the effect of multiple reflections, although having only a small influence on the reflection induced noise power, changes the distribution of the noise and has more serious system effects. In the case of a multiplicity of reflection points it is shown that for as few as four reflection points, the Gaussian approximation gives results in good agreement with results calculated from a Gram-Charlier series approximation to the actual distribution function. Power penalties as a function of reflection coefficient are calculated and compared using several different approximations for the distribution of the interferometric noise. The methodology presented, although applied specifically to reflection induced noise, is applicable to a broader class of problems in which there are other signal dependent noise phenomena.

Acknowledgements

I am grateful to Dr. Ira Jacobs, my advisor, for his guidance and constant support during the course of this thesis. Indeed, in more than one way, his encouragement enabled me to complete this work. Working with him has been a rewarding experience which I will always cherish.

Thanks are also due to Dr. R.Claus and Dr. T.Rappaport for agreeing to serve on my graduate committee. I wish to thank the Fiber and Electro-Optics Research Center at Virginia Tech for making work a pleasure and Bell Communications Research for the financial assistance it provided me.

I would also like to thank all my friends at Virginia Tech for all the great times I've had here, providing welcome relief from the strains and pressures of academia.

Lastly and most importantly, to my parents and brothers - Appa, Amma, Shankar and Satish : any words I have are superfluous and you know that.

Table of Contents

1.0 Introduction	1
2.0 Basic Theory	5
2.1 Interferometric noise from two reflections	6
2.2 Laser source characterization	9
2.3 Power spectral density of RIN	12
2.4 Integral of Relative Intensity Noise	14
3.0 System penalties	18
3.1 Introduction	18
3.2 Analysis with Gaussian approximations	21
3.3 Analysis with actual p.d.fs	27
3.4 Eye degradation approximation for RIN	29
3.5 Uniform approximation for the p.d.f of RIN	35
3.6 Quadratic approximation for the p.d.f	41
4.0 Extensions of the model	45
4.1 Combined effect of an extinction ratio and RIN	46
4.2 Effect of multiple reflections	51
4.3 Effect of a multiplicity of reflection points	55
4.4 The Gram-Charlier series approximation	66

5.0 Low frequency enhancements in the spectrum of RIN	72
5.1 Low frequency variations	73
5.2 Discussions	80
6.0 Physical modeling	82
6.1 Reflections from splices and connectors	83
6.2 Reflections from non contacting joints	84
6.3 Coding effects on RIN	88
7.0 Conclusions	90
7.1 Summary	90
7.2 Conclusions and principal contributions	91
7.3 Suggestions for future research	93
Appendix	94
References	98
Vita	101

List of Illustrations

Figure 2.1	Schematic diagram of a fiber transmission system	7
Figure 2.2	Power spectral density of RIN (theoretical and measured)	15
Figure 2.3	Normalized integral of RIN vs. $\Delta\nu \cdot \tau$	17
Figure 3.1	Schematic diagram of the cumulative distribution function of signal dependent noise	22
Figure 3.2	Power penalties vs. reflection coefficient R for p-i-n receiver and two reflection points : a) theoretical prediction using Gaussian p.d.f b) theoretical prediction using actual p.d.f	30
Figure 3.3	Cumulative distribution function of RIN approximated as an eye-degradation	32
Figure 3.4	Power penalties versus R : a) actual calculation, b) eye-degradation approximation $\epsilon = \epsilon_{\max}$, c) eye degradation approximation $\epsilon = \epsilon_{\max} - 0.03$	34
Figure 3.5	Cumulative distribution function of RIN approximated as a straight line	36
Figure 3.6	Power penalties versus reflection coefficient R : a) Gaussian distribution, b) actual distribution, c) uniform distribution with matching bounds, d) uniform distribution with matching variance	40
Figure 3.7	Power penalties vs. reflection coefficient R : a) Gaussian distribution, b) uniform distribution with matching bounds, c) quadratic distribution	43
Figure 4.1	Power penalty vs. reflection coefficient R for different values of extinction ratio $1/\epsilon$	50
Figure 4.2	Power penalty as a function of ϵ for R = 0.03 : a) Gaussian distribution for RIN, b) eye-degradation approximation for RIN	52
Figure 4.3	Power penalty vs. reflection coefficient R with RIN being approximated as eye degradation : a) single pair of reflections, b) multiple reflections	56
Figure 4.4	Power penalty vs. number of reflectors for different values of reflection coefficient R : a) R = 0.06, b) R = 0.01, c) R = 0.01 and 0.5 dB loss between adjacent reflection points	61

Figure 4.5	Power penalty vs. reflection coefficient R for 3 reflectors and different approximations for the p.d.f of RIN : a) Gaussian approximation, b) uniform approximation, c) quadratic approximation, d) Gram-Charlier series approximation	63
Figure 4.6	Power penalty vs. reflection coefficient for 4 reflectors : a) Gaussian approximation, b) uniform approximation, c) quadratic approximation d) Gram-Charlier series approximation	64
Figure 5.1	DC values of normalized power spectrum of RIN as a function of : a) $\kappa = 0$, b) $\kappa = 0.4$, c) $\kappa = 0.8$	78
Figure 5.2	σ^2 as a function of normalized time τ/τ_c for $\gamma = 1$: a) $\kappa = 0$, b) $\kappa = 0.4$, c) $\kappa = 0.8$	79
Figure 5.3	Low frequency enhancement in the power spectrum of RIN plotted vs. normalized frequency $\omega\tau_c$	81
Figure 6.1	Transmission vs. fiber end separation for a single mode fiber at a wavelength of 1300 nm	85
Figure 6.2	Concept of a double bulb connector	87
Figure 6.3	Power penalty vs. reflection coefficient R for : a) NRZ, $\tau = 40$ bits, b) RZ, $\tau = 40$ bits, c) NRZ, $\tau = 40.5$ bits, d) RZ, $\tau = 40.5$ bits	89

1.0 Introduction

The performance of single mode optical fiber systems may be affected by interference effects resulting from reflections that may occur at fiber joints such as connectors and endfaces [1]. These reflectors are essentially refractive index discontinuities along the fiber path. For example, an airgap between two connector endfaces can reflect as much as 22.4 % of the incoming power back towards the transmitter. If these reflections come back into the laser cavity, they result in a number of deleterious effects which include the shifting of the center frequency of the laser. The effects of reflections into the laser cavity are minimized by including an optical isolator in the transmitter package. This thesis considers the effects of multiple reflections within the fiber path itself. Such reflections result in a delayed signal that interferes with the direct signal. This interference phenomenon results in the conversion of laser phase noise into intensity noise.

Reflection-induced noise (also called relative intensity noise or RIN) in a fiber communications system is basically the result of interferometric conversion of the laser phase noise into intensity noise by the refractive index discontinuities in the system downstream of the isolator. The study of interferometric conversion of laser phase noise into intensity noise is not new, as the work of Armstrong [2], and Edgar and Weidel [3], to name a few, shows. However, the study of the system effects of such noise is relatively

new ([3] - [6]) and has attained increased importance as a consequence of the development of very high speed systems with bandwidths comparable to the linewidth of the laser. In prior lower bit rate systems, where the source spectral width was large compared to the bit rate, these effects are generally negligible, since the receiver filters out much of this noise. However, as the bit rate increases, and as the source linewidth decreases, the effects of this noise become more significant. Since it is difficult to avoid reflections at connectors and splices, and there may be many such discontinuities in the fiber path, this has become a major concern in the system design and physical deployment of fiber networks. Hence there is a need to understand and assess the impact of this phenomenon on the performance of fiber systems.

The intent of this thesis is two-fold. One is to examine the effects of RIN in detail, considering it as a specific impairment in a fiber optic communications system. We first present the basic theory explaining RIN and summarize results from the literature. This is for a simple model that considers only a single pair of reflectors in the system. We next extend this model to consider the effect of other impairments in the system and also generalize the theory to explain discrepancies between the theoretical predictions of the simple model and experimental results. We also generalise the theory to assess the impact of more than two such refractive index discontinuities in the system.

The second motive behind this work is to develop simple analytical models to evaluate the impact of signal-dependent noise on a general communications system. RIN is a typical example of such a noise process. We use RIN as a specific case and test the approximate methods we develop with exact calculations in special cases. The general idea behind trying these various approaches is that in many situations it is difficult to derive an exact analytical expression for the probability density function of signal dependent noise. Further, it is even more difficult to evaluate the error probability and thus the power penalty in such a situation - the integrals normally are at least two-dimensional and in general are not amenable to an analytical solution. (Power penalty is defined as the increase in signal input power required to achieve the same bit-error-rate performance of the system as in the absence of the impairment.) While numerical methods can be and have been adopted to estimate the error probability and hence the power penalty when the distribution of the

interference is known, there is some interest in trying to simplify the analysis by approximating the incompletely known probability density function by other simpler functions which may give fairly accurate results over a class of distributions. Some of these approaches are used to analyse this phenomenon of reflection induced noise and they may be extrapolated to handle a wider class of problems. Our motive is to try to gain some insight into the conditions under which different approximations may be used to model a physical noise process.

It is important to note that although it is difficult to obtain accurate estimates of the actual probability of error, power penalty is in general a less sensitive function of the shape of the pdf and may be more easily approximated. In a typical power limited fiber communication system, we are generally more interested in the power penalty caused by an impairment than in the change in the error probability at a given power level. Owing to the steepness of the error probability vs. power curves, good approximations to the power penalty may be achieved without accurate calculations of error probability.

Chapter two essentially summarizes the existing theory of RIN from the literature. The process of the interferometric conversion of the laser phase noise into intensity noise is explained, using a simple model. The mathematics describing the random variations in the laser phase are presented. Basically, the analysis is done with the laser assumed to be operating in a CW condition.

In chapter three, the impact of this noise on a fiber communications system using on-off keying is considered. The initial part of this chapter again presents results from the literature. In the latter part of the chapter, the approximations to the probability density function of RIN developed by us are presented. In this chapter, only a single pair of reflections are considered and all other impairments in the system are neglected, with the exception of the receiver thermal noise, of course.

Chapter four deals with the extensions to the basic model that are made to consider other impairments and a multiplicity of reflectors in the system. Again, the actual results computed with these extensions are used as a basis to test the results calculated with the approximations developed.

In chapter five, the unmodulated (CW) laser is considered again. We present there

the outline of a model for the laser linewidth that qualitatively explains the discrepancies in the power spectrum of RIN that have been reported between theory and experiment [6].

In chapter six, we take a closer look at the physical causes of the reflections and relate them with the parameters of the models developed.

Chapter seven includes a summary of work done, conclusions drawn and suggestions for future work.

2.0 Basic Theory

In this chapter, the theory developed in the literature ([2] - [6]) is summarised. The process of the interferometric conversion of the laser phase noise into intensity noise is explained by considering a pair of refractive index discontinuities as a Fabry-Perot interferometer. Some knowledge of the laser source modelling is imperative in understanding RIN. An outline of the model describing the random phase fluctuations of the laser source is presented. Lastly, the expressions for the autocorrelation function and the power spectral density of RIN are presented. It must be noted here that the effects of RIN are significant only in single mode systems. Even though RIN is present in a multimode fiber system, the effects of other impairments like mode-partition noise etc. are far more significant in determining overall system performance [3].

2.1 Interferometric noise from two reflections

A schematic of a fiber transmission line containing a number of refractive index discontinuities such as those occurring at connector endfaces, splices or interfaces between fiber pigtails and fiber optic components, including transmitters and receivers is indicated in Fig. 2.1 [6]. These interfaces constitute a number of Fabry-Perot interferometers which convert the laser phase noise into excess intensity noise.

The Fabry-Perot interferometer formed by two discontinuities is considered first. The characteristics of the interferometer are determined by the intensity reflection coefficients R_1 and R_2 , the round trip delay time τ , and the single pass intensity transmittance α . The delay time τ equals $2nd / c$ where d is the distance between the discontinuities, n is the refractive index of the fiber and c is the speed of light in free space. The laser is assumed to be operating under continuous wave (CW) condition, for which the input optical field into the interferometer is described as [7]:

$$e_i(t) = E_0 \exp(j\omega_0 t + \varphi(t)) + c.c \quad (2.1.1)$$

where E_0 is the field amplitude, ω_0 is the laser center frequency, $\varphi(t)$ is the random phase which contains all deviations from a monochromatic wave. This is explained in more detail in the next section. The output of the interferometer may be approximated as the combination of a direct and a doubly reflected field :

$$e(t) = \sqrt{\alpha} e_i(t) + \alpha^{3/2} \sqrt{R_1 R_2} e_i(t - \tau) + c.c. \quad (2.1.2)$$

The reflection coefficients have been assumed to be sufficiently small so that terms of the order $(R_1 R_2)$ and higher have been neglected. It is also assumed here that the doubly reflected field is polarized in the same direction as the incident field. The intensity $I(t) = |e(t)|^2$ is detected at the receiver. From equation (2.1.2) the expression for $I(t)$ can be written as :

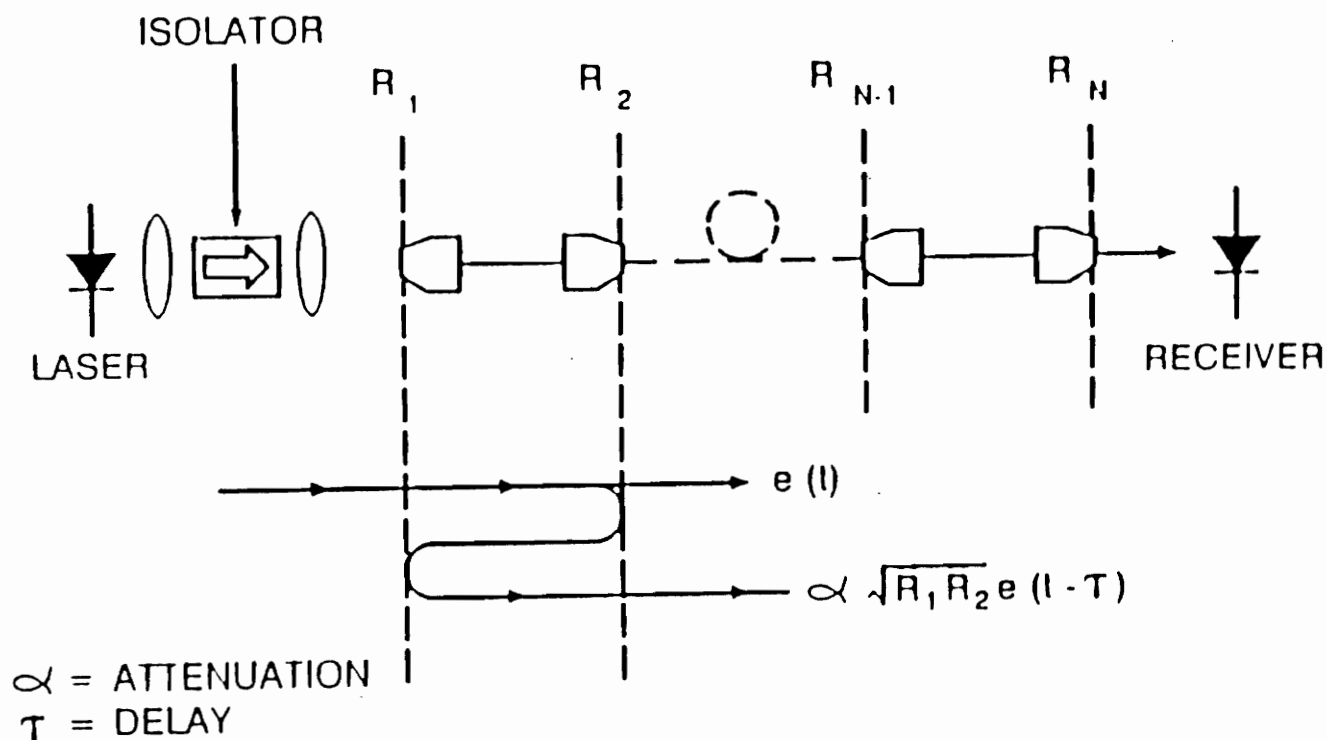


Fig. 2.1

Schematic diagram of a fiber transmission system with multiple reflection points : an illustration of interference generated between a pair of optical discontinuities. (taken from ref.[6])

$$I(t) = \alpha E_0^2 \left| \left[\exp(j(\omega_0 t + \varphi(t))) + R \exp(j(\omega_0(t - \tau) + \varphi(t - \tau))) + \exp(-j(\omega_0 t + \varphi(t))) + R \exp(-j(\omega_0(t - \tau) + \varphi(t - \tau))) \right] \right|^2 \quad (2.1.3)$$

When taking the magnitude squared of the right hand side of eq.(2.1.3), terms with frequency ω_0 and $2\omega_0$ are neglected since they are filtered out by the detector. Here, R is an effective reflection coefficient which depends upon the transmittance factor α and polarization alignment of the two interfering fields as well as the reflection coefficients R_1 and R_2 :

$$R = \alpha \sqrt{R_1 R_2} \quad (2.1.4)$$

The fields are, of course, vector fields and the above assumes that they are parallel. In practice, there may be some depolarization in the reflections in which case R will further be reduced. Further, as indicated by eq.(2.1.1), amplitude fluctuations of the laser source have been assumed to be negligible (explained in the next section). Equation (2.1.3) can be written as

$$I(t) = \alpha E_0^2 [1 + \rho(t, \tau)] \quad (2.1.5)$$

where $\rho(t, \tau)$ is the interference term given by :

$$\rho(t, \tau) = 2R \cos(\omega_0 \tau + \Phi(t, \tau)) \quad (2.1.6)$$

Throughout this thesis, it is assumed that the transmittance $\alpha = 1$ i.e. losses are neglected (unless explicitly stated otherwise). The phase noise variable in this equation is defined as follows :

$$\Phi(t, \tau) = \varphi(t) - \varphi(t - \tau) \quad (2.1.7)$$

To develop a better understanding of the equations developed so far, a brief outline on laser

source characterization is presented next.

2.2 Laser source characterization

In general, the emission field of optical sources vary with time in a random fashion and are therefore statistical in nature [8]. This randomness can have either a quantum origin, generated inside the cavity or it may be due to external random perturbations. For a given polarization state, the emission field fluctuates randomly, in both phase and amplitude with a possible correlation between them. However, due to the damping of the amplitude fluctuations by gain saturation, semiconductor laser sources operating well above threshold exhibit negligible intensity fluctuation at or near the lasing frequency. As a result, the dominant contribution to the line broadening comes from the randomness of the quantum phase fluctuations which are primarily caused by spontaneous emissions within the laser cavity. Hence, the emission field for a single longitudinal mode of the laser source can be described by :

$$e(t) = E_0 \exp(j(\omega_0 t + \varphi(t))) \quad (2.2.1)$$

with E_0 as the instantaneous amplitude which is assumed to be constant, ω_0 the center frequency and $\varphi(t)$ the time varying phase of the laser.

The phase is usually assumed to undergo a random walk process [9]. More specifically, it is a common assumption to take the Wiener-Levy random process as a statistical model for the random phase fluctuations of the laser light. This model explains many of the important properties involving the phase.

According to the Wiener-Levy model [10], the phase itself is a non-stationary zero mean Gaussian random process whose autocorrelation function is given by :

$$\langle \varphi(t_1) \cdot \varphi(t_2) \rangle = \xi \min(t_1, t_2) \quad (2.2.1)$$

where t_1 and t_2 are two arbitrary time instants, “min” denotes the smaller of the arguments and ξ is a proportionality constant determined by the particular physics of the process being considered. In addition, the Wiener-Levy process has the important property that although the process itself is non-stationary, the first increments are stationary and independent. The first increment is nothing but the phase difference :

$$\Phi(t, \tau) = \varphi(t) - \varphi(t - \tau) \quad (2.2.2)$$

Hence, $\Phi(t, \tau)$ is also a zero-mean Gaussian process, with a probability density function given by :

$$p_{\Phi}(\Phi) = \frac{1}{\sigma(\tau)\sqrt{2\pi}} \exp\left(-\frac{\Phi^2}{2\sigma^2(\tau)}\right) \quad (2.2.3)$$

The variance $\sigma^2(\tau)$ is given by :

$$\sigma^2(\tau) = \langle (\varphi(t) - \varphi(t - \tau))^2 \rangle$$

Using eq.(2.2.1), this is evaluated to give :

$$\begin{aligned} \sigma^2(\tau) &= t\xi + (t - \tau)\xi - 2\xi \min(t, t - \tau) \\ &= \xi |\tau| \end{aligned} \quad (2.2.4)$$

The coherence time of the laser is defined by :

$$\sigma^2(\tau) = \frac{|\tau|}{\tau_c} \quad (2.2.5)$$

Hence,

$$\xi = \frac{1}{\tau_c} \quad (2.2.6)$$

It is readily shown that the power spectrum of the field emitted by the laser is given by :

$$P(f) = \frac{E_0^2 \Delta\nu}{(f - f_0)^2 + \left(\frac{\Delta\nu}{2}\right)^2}$$

where

$$\Delta\nu = \frac{1}{2\pi\tau_c} \quad (2.2.7)$$

Note that $\Delta\nu$ is the full width half maximum (FWHM) linewidth of the laser and f_0 is the center frequency of the laser. This corresponds to a laser power spectral density function having a Lorentzian line shape. In the development of these expressions, the effects of relaxation oscillations on the laser lineshape have been neglected. Using these formulas, the autocorrelation and the power spectral density of the interference term $\rho(t, \tau)$ are evaluated in the next section. The Wiener-Levy model is equivalent to assuming that the instantaneous frequency fluctuations $\dot{\phi}(t)$ are a white noise Gaussian process. In practice, high frequency phenomena (relaxation oscillations) affect the spectral line shape [11], and as will be shown in chapter five, low frequency thermal phenomena may also affect the spectral shape of RIN.

2.3 Power spectral density of RIN :

The interference term $\rho(t, \tau)$ defined in eq.(2.1.6) shows how the random fluctuations in phase are converted into intensity fluctuations called Relative Intensity Noise (RIN). The noise spectral density is calculated from the Fourier transform of the autocorrelation function $R(t, \tau)$:

$$\begin{aligned} R(t, \tau) &= \langle \rho(t_1, \tau) \cdot \rho(t_1 + t, \tau) \rangle \\ &= E [\rho(t_1, \tau) \cdot \rho(t_1 + t, \tau)] \end{aligned} \quad (2.3.1)$$

Time averages are equated to ensemble averages since the process is assumed to be ergodic. The autocorrelation function $R(t, \tau)$ is then given by :

$$\begin{aligned} R(t, \tau) &= E [\{ R \exp(j(\omega_0 \tau + \varphi(t_1) - \varphi(t_1 - \tau))) + R \exp(-j(\omega_0 \tau + \varphi(t_1) - \varphi(t_1 - \tau))) \} \cdot \\ &\quad \{ R \exp(j(\omega_0 \tau + \varphi(t_1 + t) - \varphi(t_1 + t - \tau))) + R \exp(-j(\omega_0 \tau + \varphi(t_1 + t) - \varphi(t_1 + t - \tau))) \}] \end{aligned} \quad (2.3.2)$$

$$\begin{aligned} &= E [R^2 \exp(j(\omega_0 \tau + \varphi(t_1) - \varphi(t_1 - \tau) + \varphi(t_1 + t) - \varphi(t_1 + t - \tau))) \\ &\quad + R^2 \exp(j(\varphi(t_1 + t) - \varphi(t_1 + t - \tau) - \varphi(t_1) + \varphi(t_1 - \tau)))] + \text{c.c.} \end{aligned} \quad (2.3.3)$$

These random variables $\rho(t_1, \tau)$ and $\rho(t_1 + t, \tau)$ are statistically independent if the time intervals over which the phase difference is taken are disjoint [7]. Noting further that :

$$E [\exp(j(\varphi(t) - \varphi(t - \tau)))] = \exp(-\frac{\sigma^2}{2}) \quad (2.3.4)$$

the autocorrelation function can be easily evaluated to give :

$$R(t, \tau) = 2R^2 \begin{cases} \exp(-2\pi\Delta\nu|t|)[1 + \cos 2\omega_0\tau \cdot \exp(-4\pi\Delta\nu(\tau - |t|))], & |t| < \tau \\ \exp(-2\pi\Delta\nu\tau) [1 + \cos 2\omega_0\tau] & |t| > \tau \end{cases} \quad (2.3.5)$$

The power spectral density is obtained by taking the Fourier transform of $R(t, \tau)$:

$$RIN(f) = \int_{-\infty}^{\infty} R(t, \tau) \exp(-j\omega t) dt \quad (2.3.6)$$

After subtracting the d.c. term, $RIN(f)$ is found to be :

$$RIN(f) = \frac{4R^2}{\pi} \left[\frac{\Delta\nu}{f^2 + (\Delta\nu)^2} \right] \cdot \left\{ \sin^2(\omega_0\tau) \cdot [1 + e^{-4\pi\Delta\nu\tau} - 2e^{-2\pi\Delta\nu\tau} \cos 2\pi f\tau] \right. \\ \left. + \cos^2(\omega_0\tau) \cdot [1 - e^{-4\pi\Delta\nu\tau} - 2e^{-2\pi\Delta\nu\tau} \frac{\Delta\nu}{f} \sin 2\pi f\tau] \right\} \quad (2.3.7)$$

From this expression, it can be shown that the maximum conversion of phase noise to intensity noise occurs when the direct and doubly reflected fields interfere in quadrature, i.e.

$$\omega_0\tau = (n + \frac{1}{2})\pi \quad (2.3.8)$$

For this case, in the limit of $2\pi\Delta\nu\tau \ll 1$,

$$RIN(f) \rightarrow \frac{16}{\pi} R^2 \Delta\nu \tau^2 \text{sinc}^2 f\tau \quad (2.3.9)$$

Thus, in the limit of small phase fluctuations, RIN is proportional to $\Delta\nu$. In this limit, very narrow linewidth lasers exhibit less interferometric intensity noise. However, for longer delay paths τ , with $2\pi\Delta\nu\tau \gg 1$, the interfering terms combine incoherently. For this case, $RIN(f)$ approaches a functional dependence given by :

$$RIN(f) \approx \frac{4R^2}{\pi} \left[\frac{\Delta\nu}{f^2 + (\Delta\nu)^2} \right], \quad (2\pi\Delta\nu\tau \gg 1) \quad (2.3.10)$$

independent of the phase offset $\omega_0\tau$. Eq.(2.3.7) is plotted [6] and is shown in Fig. (2.2) for $R_1 = R_2 = 6\%$, $\Delta\nu = 43$ MHz, and the delay $\tau = 50$ ns. It is generally the incoherent case that is encountered in practice. In the above example, $2\pi\Delta\nu\tau = 13.5$. A delay of 50ns corresponds to a distance between reflectors of 5 meters, not atypical for fiber jumpers.

2.4 Integral of Relative Intensity Noise :

From eq.(2.3.7), it is seen that the interferometric noise is frequency dependent and is proportional to signal power. The impact of this noise on system performance will depend on the total integral of $RIN(f)$ over receiver bandwidth. For very wide linewidth sources such as LEDs, the power spectral density of the intensity noise is small, as is the integrated noise power. For low speed systems, the receiver bandwidth too is small and most of the noise is filtered out. For high bit rate systems however, where the system bandwidth is substantially greater than the source linewidth, the integral of RIN can be large, substantially impacting system performance. It can be seen that $RIN(f)$ decreases

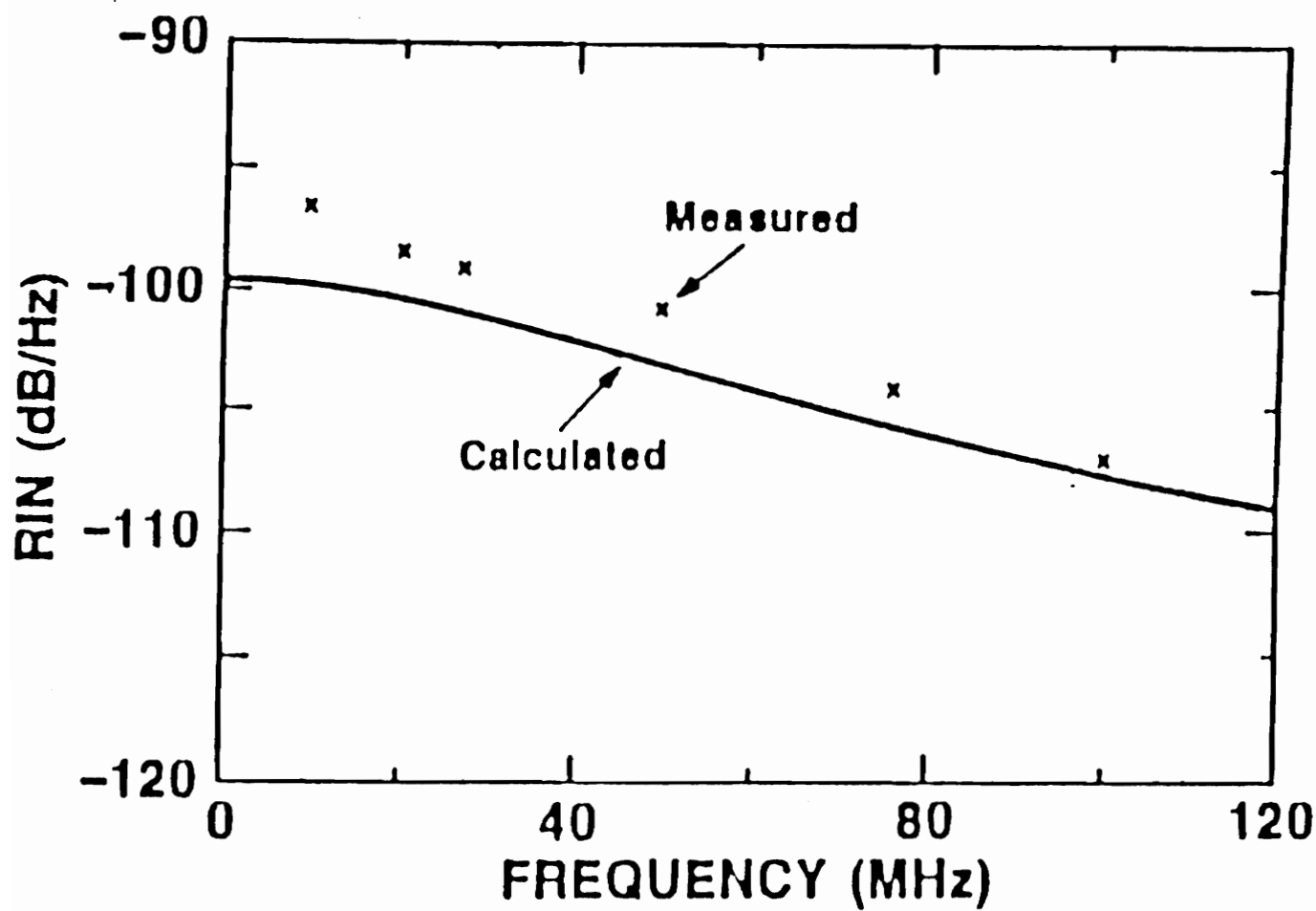


Fig. 2.2 Power spectral density of RIN (theoretical and measured)
(taken from ref.[6])

rapidly for $f \gg \Delta\nu$. In fact, in the incoherent case ($2\pi\Delta\nu \tau \gg 1$), over 90 % of the noise power is contained in the frequency band $0 < f < 6.3 \Delta\nu$. In the high bit rate case,

$$\delta^2 = \int_0^\infty \text{RIN}(f) df \quad (2.4.1)$$

$$= 2R^2 \begin{cases} 1 - \exp(-4\pi\Delta\nu\tau), & \omega_0\tau = (n + \frac{1}{2})\pi \\ 1 + \exp(-4\pi\Delta\nu\tau) - \exp(-2\pi\Delta\nu\tau), & \omega_0\tau = n\pi \end{cases} \quad (2.4.2)$$

The normalized integral $\delta^2 / 2R^2$ is plotted in Fig.(2.3) for the two cases mentioned in eq.(2.4.2) corresponding to the phases of the direct and doubly reflected fields interfering in quadrature and in phase respectively. For both cases, the integral of RIN rapidly approaches a value of $2R^2$ when $\Delta\nu\tau \geq 1$, corresponding to incoherent interference. This is the condition most generally encountered in present DFB laser direct detection schemes.

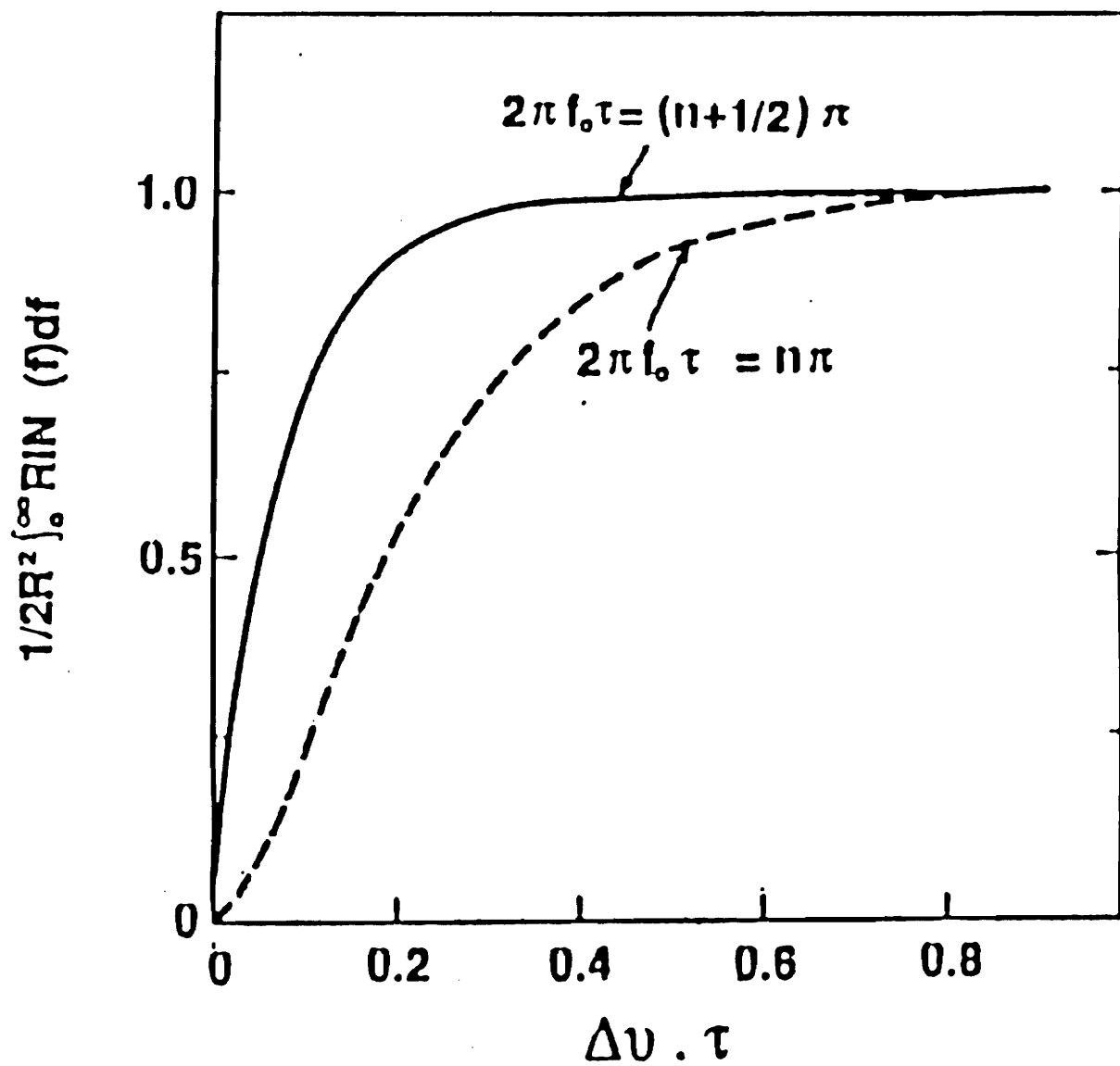


Fig. 2.3 Normalized integral of RIN vs. $\Delta\nu \cdot \tau$
(taken from ref.[6])

3.0 System Penalties

3.1 Introduction

Interferometric intensity noise is a signal dependent noise which can lead to performance degradations in fiber systems, and can even cause bit error ratio (BER) floors. A BER floor is said to occur when the error probability asymptotes towards a non-zero value. Even arbitrarily large increases in the input signal power do not result in lower error rates. In chapter 2, the noise spectral density of RIN was calculated for the case of an unmodulated laser. To estimate system penalties resulting from interferometric noise, a typical fiber transmission system based upon binary on-off keying (OOK) of the laser transmitter is considered. Non-return-to-zero (NRZ) formatted data is considered, with the laser pulse waveform for an isolated “one” given by :

$$\begin{aligned} a(t) &= 1, & 0 < t < T \\ &= 0, & \text{otherwise} \end{aligned} \quad (3.1.1)$$

where T is the bit duration. Other line coding schemes influence the statistics of RIN differently. This is discussed in greater detail in chapter six. In the case of two reflectors,

i.e. one reflection term, the electrical current at the receiver, which is proportional to the optical intensity, is given by :

$$i(t) = \{ E_0^2 [a(t) + v(t)] + n(t) \} \oplus h_r(t) \quad (3.1.2)$$

where proportionality factors are suppressed, $h_r(t)$ is the receiver impulse response function and $v(t)$ is the RIN term given by :

$$v(t) = 2 \sqrt{a(t) a(t - \tau)} R \cos (\omega_0 \tau + \Phi(t, \tau)) \quad (3.1.3)$$

(see eq. (2.1.6)) Here, $n(t)$ is an additional noise term that represents the receiver thermal noise.

The interference term $v(t)$ depends upon the product $a(t) \cdot a(t - \tau)$ and therefore upon the data sequence. Only very high bit rate systems and narrow linewidth sources are considered so that all of the interferometric noise is assumed to fall within the receiver bandwidth. Hence the effect of the receiver impulse response function will not be considered any further in the analysis. Further, only the case of incoherent interference is considered, for which the argument of the cosine function in eq.(3.1.3), $(\omega_0 \tau + \Phi(t, \tau))$, may be treated as a uniformly distributed random variable. As will be shown later, the probability density function (pdf) of the interferometric noise is distinctly non-Gaussian. Nevertheless, in order to compute power penalties from this noise, it is convenient to approximate the noise as having a Gaussian pdf. This approximation leads to a closed form expression for the power penalty, and for small penalties provides relatively good estimates (determined by comparison with actual penalty). However, in order to compute large performance degradations or BER floors, the actual pdf should be used. The analysis has been carried out using both pdfs and is presented in the next two sections.

The remainder of this chapter deals with the various approximations to the distribution of the interferometric noise made for reasons explained in chapter 1.

The signal at the receiver decision point may be written in the following general form :

$$y = a + xRa + n \quad (3.1.4)$$

where R is the reflection coefficient, n is the signal independent Gaussian noise, and x is the random variable representing the interferometric noise in the on-state. This formalism incorporates all the randomness of the phenomenon into the variable x which is independent of R and a . It will be assumed that the decision threshold is set at the value in the absence of signal dependent noise ($a/2$), although some improvement in performance may be achieved [13] by adjusting the threshold if the statistics of the signal dependent noise are known. This is discussed further in section 4.1. The noise is assymmetric and therefore the errors are dominated by those in the on-state. The error probability can then be expressed as :

$$\begin{aligned} P_E &= \text{prob.} \left\{ xRa + n < -\frac{a}{2} \right\} \\ &= \text{prob.} \left\{ x > \frac{1}{2R} \left(1 - \frac{2n/\sigma}{a/\sigma} \right) \right\} \end{aligned} \quad (3.1.5)$$

where σ^2 is the variance of the thermal noise. Or,

$$P_E = \frac{1}{\sqrt{2\pi}} \int_{-\infty}^{\infty} du \exp\left(-\frac{u^2}{2}\right) F \left\{ \frac{1}{2aR} \left(1 - \frac{u}{\alpha} \right) \right\} \quad (3.1.6)$$

where $\alpha = a / 2\sigma$ is the signal to thermal noise amplitude ratio, $u = n / \sigma$ represents a zero mean unit variance Gaussian random variable and

$$F(\xi) = \int_{\xi}^{\infty} dx p(x) = \text{prob.}(x > \xi) \quad (3.1.7)$$

i.e $F(-\infty) = 1$, $F(0) = 1/2$, $F(\infty) = 0$. This is depicted graphically in fig.(3.1).

For $R = 0$, P_E is given by the integral of the tail of the Gaussian distribution. For $R \neq 0$, P_E is given by the integral of the product of F and the p.d.f of the zero-mean unit variance Gaussian distribution. Clearly, P_E is critically dependent on the tail of F extending towards the peak of the Gaussian.

Basically, in each of these next sections, the random variable x is approximated differently.

3.2 Analysis with Gaussian approximations :

The received signal is of the form :

$$y(t) = a(t) + xRa(t) + n(t) \quad (3.2.1)$$

where $a(t)$ is given by eq.(3.1.1), $x(t)$ is the noise term assumed to have a Gaussian distribution, and $n(t)$ is the thermal noise term, which is a zero mean Gaussian process.

Let μ_1 and μ_0 denote the expectation values, and σ_1^2 and σ_0^2 the noise variances of the signal $y(t)$ for "ones" and "zeros" respectively. Let D be the decision threshold to which $y(t)$ is compared.

The decision rule is then given by [12] :

choose hypothesis H_0 ($a(t) = 0$) if $y < D$,
choose hypothesis H_1 ($a(t) = 1$) if $y > D$,

The probability that the decision will be in error (i.e. the error probability) P_E is

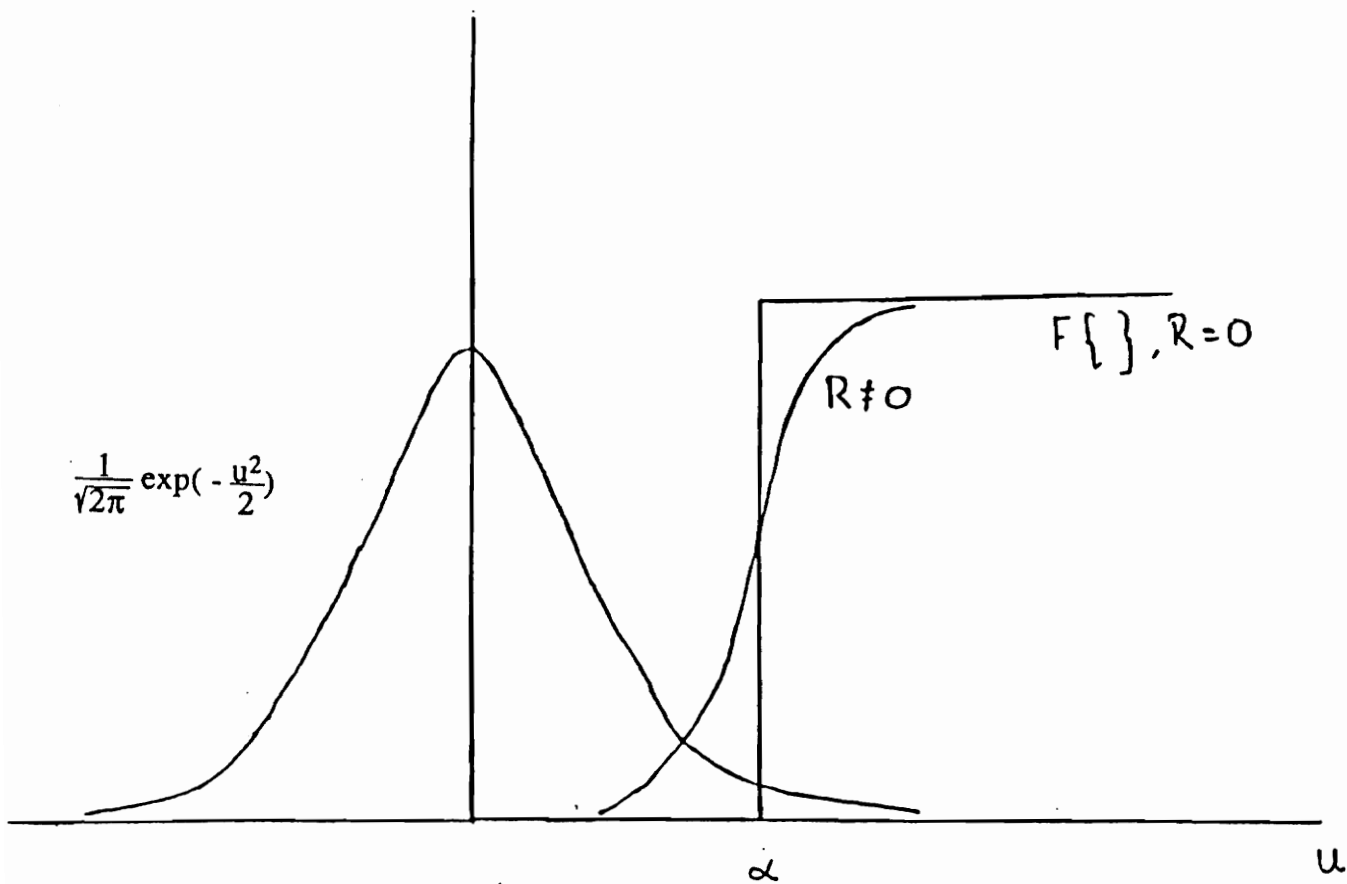


Fig. 3.1 Schematic diagram of the cumulative distribution function of signal dependent noise

then given by :

$$P_E = \frac{1}{2} \text{prob.} \{ v + n < D \mid H_1 \} + \frac{1}{2} \text{prob.} \{ v + n > D \mid H_0 \} \quad (3.2.2)$$

where it is assumed that there is equal (1/2) probability for transmitting a zero and a one.

For Gaussian - distributed noise, the probability of error can be expressed as :

$$P_E = \frac{1}{2} Q\left(\frac{\mu_1 - D}{\sigma_1}\right) + \frac{1}{2} Q\left(\frac{D - \mu_0}{\sigma_0}\right) \quad (3.2.3)$$

where :

$$Q(\chi) = \int_{\chi}^{\infty} \frac{1}{\sqrt{2\pi}} \exp\left(-\frac{x^2}{2}\right) dx \quad (3.2.4)$$

The shot noise due to the signal itself is negligible for PIN receivers. In the absence of other signal dependent noise sources, the noise variances for $y(t)$ are the same for both “ones” and “zeros” :

$$\sigma_1^2 = \sigma_0^2 = \langle n^2 \rangle \quad (3.2.5)$$

where $\langle n^2 \rangle$ is the variance of the thermal noise. The optimum decision level is then midway between the expectations μ_1 and μ_0 . For the case where there is no intersymbol interference :

$$\mu_0 = 0, \quad \mu_1 = E_0^2, \quad D = \frac{\mu_1}{2} \quad (3.2.6)$$

The interferometric noise represented by x in eq.(3.1.3) affects only the “1” bits. Assuming

that the threshold is not reoptimized, i.e. $D = \mu_1/2$ even in the presence of the interferometric noise, the probability of error P_E is given by :

$$P_E = \frac{1}{2} Q\left(\frac{\mu_1}{2\sigma_1}\right) + \frac{1}{2} Q\left(\frac{\mu_1}{2\sigma_0}\right) \quad (3.2.7)$$

The case of reoptimized thresholds is discussed in [13]. The noise variance σ_1^2 for “ones” can be determined from equations (3.1.2) and (3.1.3) as follows :

$$\begin{aligned} \langle y \rangle &= \mu_1, \\ \sigma_1^2 &= \langle y^2 \rangle - \langle y \rangle^2 \\ &= \left\langle \left(E_0^2 (a(t) + 2 \sqrt{a(t) a(t-\tau)} R \cos(\omega_0 \tau + \Phi(t, \tau))) \right)^2 \right\rangle \end{aligned} \quad (3.2.8)$$

Now, $\langle \cos^2(.) \rangle = 0.5$. Further, successive symbols are assumed to be independent because the time delay τ is assumed to be fairly large (corresponding to incoherent interference) so that :

$$\langle a(t) a(t-\tau) \rangle = \langle a(t-\tau) \rangle = \frac{1}{2} \quad (3.2.9)$$

since $a(t) = 1$ only. Hence σ_1^2 can be written as :

$$\begin{aligned} \sigma_1^2 &= \sigma_0^2 + 2E_0^4 \langle a(t-\tau) \rangle \langle R^2 \rangle \\ &= \sigma_0^2 + \mu_1^2 \langle R^2 \rangle \end{aligned} \quad (3.2.10)$$

For moderate power penalties, P_E will be dominated by the first term in eq.(3.2.7) (the error term due to “ones”). From eq.(3.2.7) and (3.2.10), the power penalty incurred in maintaining a probability of error = 10^{-9} is determined as follows :

$$P_E = \frac{1}{2} Q\left(\frac{\mu_1}{2\sigma_1}\right) = 10^{-9} \quad (3.2.11)$$

Let

$$\frac{\mu_1}{2\sigma_1} = k$$

where k is such that $Q(k) = 2 \cdot 10^{-9}$. The value of k which satisfies this equation is found from standard statistical tables and approximately equals 6.0. From eq. (3.2.10),

$$\frac{\mu_1}{2\sqrt{\sigma_0^2 + \mu_1^2 \langle R^2 \rangle}} = k \quad (3.2.12)$$

or, after some algebra,

$$\frac{\mu_1^2}{4\sigma_0^2} = \frac{k^2}{1 - 4k^2 \langle R^2 \rangle} \quad (3.2.13)$$

The power penalty P is defined to be the increase in optical signal power necessary to maintain a given error probability (10^{-9} in this case) :

$$\begin{aligned}
P &= 10 \log \left(\frac{\mu_1(R)}{\mu_1(0)} \right) \\
&= 10 \log \frac{1}{\sqrt{1 - 4k^2 \langle R^2 \rangle}} \\
&= -5 \log (1 - 4k^2 \langle R^2 \rangle) \\
&= -5 \log (1 - 144 \langle R^2 \rangle)
\end{aligned} \tag{3.2.14}$$

for $k = 6.0$.

If the decision threshold is reoptimized, i.e. no longer fixed at $\mu_1/2$, it can be shown that the power penalty is given by [13]:

$$P = -10 \log (1 - 36 \langle R^2 \rangle) \tag{3.2.15}$$

The quantity $\langle R^2 \rangle$ is the expectation of R^2 defined in eq. (2.1.4). If the loss between the two reflection points is minimal, as assumed, and the polarizations of the direct and doubly reflected fields are aligned, then :

$$\langle R^2 \rangle^{1/2} = \sqrt{R_1 R_2} \tag{3.2.16}$$

For randomly aligned polarization states and arbitrary transmittance β ,

$$\langle R^2 \rangle^{1/2} = \frac{1}{2} \beta \sqrt{R_1 R_2} \tag{3.2.17}$$

An examination of eq. (3.2.14) reveals that it predicts an infinite power penalty i.e. a BER floor at 10^{-9} for :

$$\langle R^2 \rangle^{1/2} = 8.5 \%$$

which gives some idea as to the maximum allowable reflectivities in systems. The dependence of reflection coefficient on physical parameters of splices and connectors is discussed in chapter six.

3.3 Analysis with actual pdfs :

Although the Gaussian approximation is useful in that it simplifies the analysis, produces closed form expressions for the power penalties and even provides good estimates for small penalties, it is not useful in estimating BER floors. The Gaussian approximation is a pessimistic one because of the infinite tail. However, as will be shown, the pdf of the interferometric noise does not extend to infinity, in fact it is sharply bounded by the limits ± 2 for the case of a single pair of reflectors. The expression for the pdf of the interferometric noise is derived below.

The interferometric noise term is given by eq. (2.1.6) :

$$x(t) = 2 \cos (\omega_0 t + \Phi(t, \tau)) \quad (3.3.1)$$

where $\Phi(t, \tau)$ is the difference in the phase at times t and $t-\tau$ respectively (described by eq.(2.1.7)) and recognising the fact that R has been decoupled from x . Assuming incoherent interference, $\Phi(t, \tau)$ is taken to be a random variable uniformly distributed over $[-\pi, \pi]$ so that $\psi(t) = \omega_0 t + \Phi$ is also uniformly distributed. The p.d.f of x is calculated as follows :

$$\begin{aligned}\psi(t, \tau) &= \cos^{-1} \frac{x}{2} \\ &= g(x)\end{aligned}\tag{3.3.2}$$

Hence, from basic probability theory [10],

$$\begin{aligned}p_X(x) &= \frac{p(\psi)}{\left| \frac{\partial g}{\partial x} \right|} \\ &= \frac{1}{\pi \sqrt{4 - x^2}}\end{aligned}\tag{3.3.3}$$

Hence, the interferometric noise is distinctly non-Gaussian - it is bounded and has maximum probability of being at one of the two extremes ± 2 . The probability of making a decision error is written as an expectation over conditional probabilities [6] i.e.

$$P_E = E \left[P_c (d_s, \tau, \Phi) \right]\tag{3.3.3}$$

where d_s (the signal data sequence), Φ and τ are the random parameters. The receiver filtering process is approximated as an integration over one bit interval and so the conditional probability P_c depends on one bit of the direct sequence and at most two bits of the delayed sequence $a(t - \tau)$ and is given by :

$$P_c = Q \left[\frac{\mu_1}{2 \sigma_0} (1 + 4R a_{ijk} \cos \Phi) \right]\tag{3.3.4}$$

where $i = 0$ or 1 denotes the direct pulse, j and $k = 0$ or 1 denotes the two overlapping delayed pulses. The random parameters a_{ijk} are determined as follows :

τ_n represents the offset time of the clocks of the direct and delayed data sequences normalized to the bit duration.

$$a_{ijk} = \sqrt{a(t) a(t - \tau)} \oplus h_r(t) \quad :$$

$$a_{0jk} = 0 \quad ; \quad a_{100} = 0 \quad ; \quad a_{110} = \tau_n \quad ;$$

$$a_{101} = (1 - \tau_n) \quad ; \quad a_{111} = 1.$$

Considering all possible combinations, the probability of error is given by :

$$P_E = \frac{1}{8} \sum_{i,j,k=0}^1 \frac{1}{2\pi} \int_{-\pi}^{\pi} d\Phi \int_0^1 d\tau_n Q \left[\frac{\mu_1}{2\sigma_0} (1 + 4R_{ijk} \cos \Phi) \right] \quad (3.3.5)$$

Power penalties as a function of R have been evaluated numerically [6], by determining for non-zero R the increase in signal power required to produce the same error probability as achieved when R = 0. Power penalties computed using both the Gaussian and the actual pdfs are plotted in Fig (3.2) for comparison. It is evident that the the Gaussian approximation is increasingly pessimistic for larger power penalties.

3.4 Eye degradation approximation for RIN :

The considerable literature on the calculation of error probability in the presence of intersymbol interference (ISI) is applicable to the problem at hand if reflections are considered to be a form of ISI. The effects of ISI are normally explained by an eye diagram

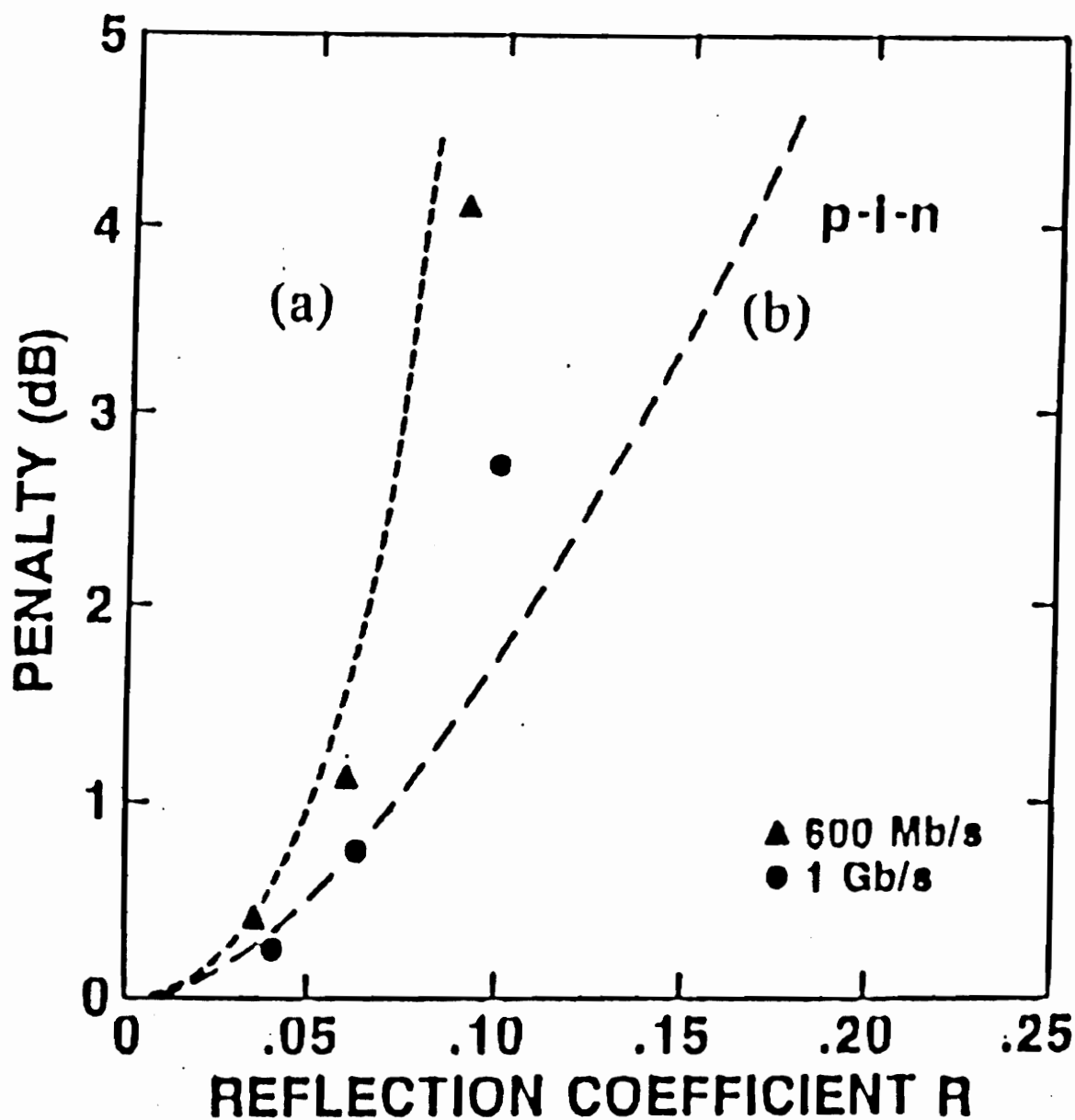


Fig. 3.2

Power penalties versus reflection coefficient R for p-i-n receiver and two reflection points :
 a) theoretical prediction using Gaussian p.d.f
 b) theoretical prediction using actual p.d.f
 (taken from ref.[6])

and the amount of degradation due to the ISI is represented by the size of the eye opening. A binary communications system is seen to have an error floor if there is a non-zero probability that the eye is closed. Basically, the performance of the system will never be better than this probability (this is an alternate way of saying that there is an error floor). If this probability equals zero, then an upper bound to P_e (which in turn gives an upper bound to the power penalty P) is obtained by considering the worst case situation in which the eye degradation equals its maximum value. This is termed the “eye degradation” approximation. In terms of the mathematical formalism developed in section 3.1, the pdf of RIN is a delta function. The corresponding cumulative distribution function is sketched in fig.(3.3). There seems to be further reason to make such an approximation because the interferometric noise is bounded and has a maximum probability of being at one of the two extremes. Note that while this is true for two reflectors, it is not true in general.

Let ϵ be the fixed eye degradation. Then, if y is the received signal,

$$\begin{aligned} y &= a - \epsilon a + n \\ &= a(1 - \epsilon) + n \end{aligned} \quad (3.4.1)$$

Assuming, as before, unipolar line symbols, the decision is set at $D = a / 2$. Then,

$$P_E = \frac{1}{2} Q \left(\frac{\mu_1 - D}{\sigma_1} \right) + \frac{1}{2} Q \left(\frac{D - \mu_0}{\mu_0} \right)$$

Now, $\mu_1 = a(1 - \epsilon)$; $\mu_0 = 0$;

$\sigma_1 = \sigma_0 = \langle n^2 \rangle$. Hence,

$$P_E = \frac{1}{2} Q \left(\frac{a(1 - \epsilon) - \frac{a}{2}}{\sigma_0} \right) = \frac{1}{2} Q \left(\frac{\frac{a}{2}(1 - 2\epsilon)}{2\sigma_1} \right) \quad (3.4.2)$$

The power penalty is then approximately equal to $-10 \log (1 - 2\epsilon)$.

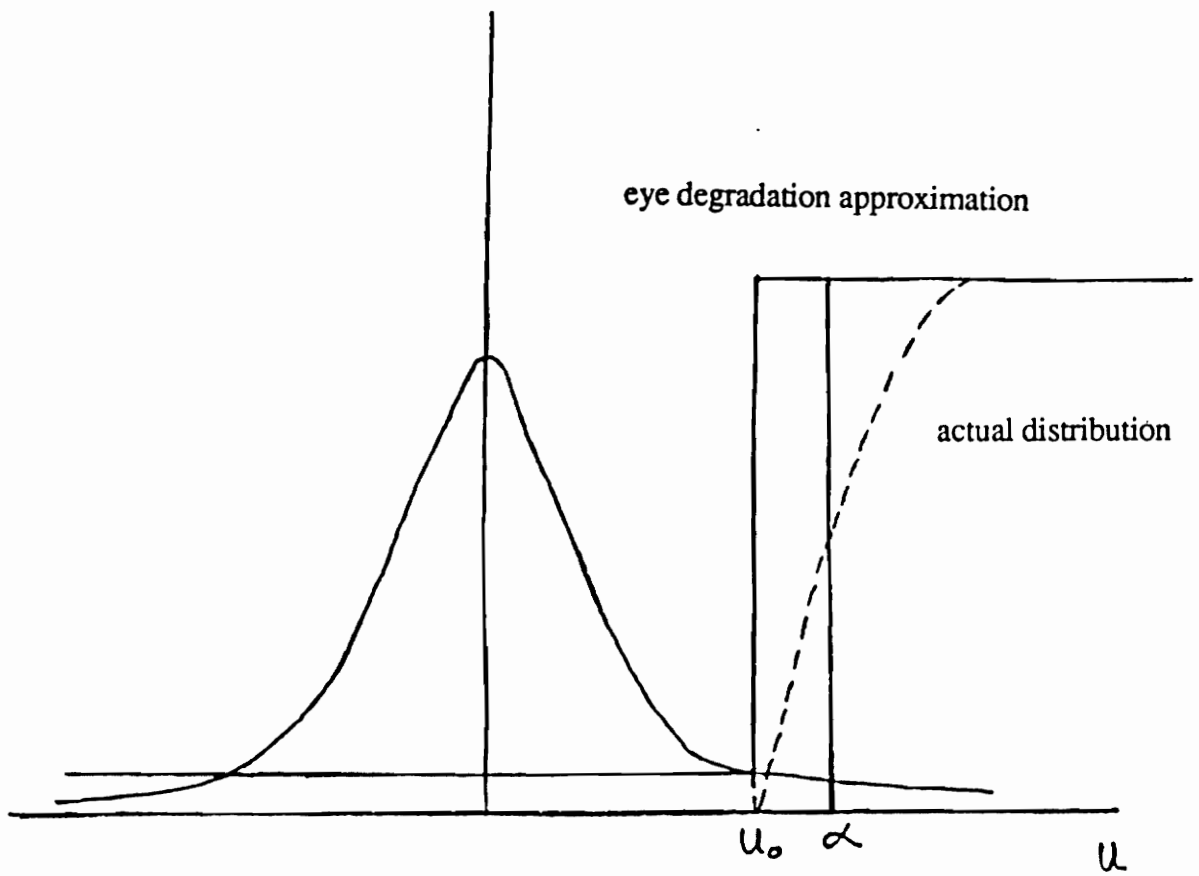


Fig. 3.3 Cumulative distribution function of RIN approximated as an eye-degradation

When $\epsilon = 2R$, the power penalty

$$= -10 \log (1 - 4 R) \quad (3.4.3)$$

This has been plotted in Fig (3.4).

It is seen from the figure that the eye degradation approximation results in slightly higher power penalties as compared to the actual distribution. However, it does provide much better estimates than the Gaussian approximation does. This appears to be a consequence of the fact that the pdf is bounded and rises extremely steeply at the extremes.

Seeing that the eye degradation approximation of $\epsilon = 2R$ provides a good estimate of the power penalty, but does not provide an exact match, there was some interest in finding out what sort of relationship between the eye degradation and the reflection coefficient R would result in power penalties that match the actual results exactly. A fourth order polynomial gave the best fit :

$$\epsilon_{\text{eff}} = 0.00018 - 0.4549 R + 41.611R^2 - 25.6754 R^3 + 514.0146 R^4 \quad (3.4.4)$$

However, a much more interesting fit was a linear one :

$$\epsilon_{\text{eff}} = -0.0308 + 2.0211 R \quad (3.4.5)$$

This fit was very poor at very small values of R (in fact, the model breaks down for $R < 0.03 / 2.02$). The power penalty has been plotted again in fig. (3.4) using this approximation. Comparing with the actual results, it is seen that there is very little difference between the two. This is an interesting result - an interferometric noise having a bounded probability density function can be approximated by an effective eye degradation which is linearly related to the maximum value of the interferometric noise.

The idea behind trying this curve fitting approach is to see if there is any simple relationship between the cumulative distribution function of the signal dependent noise and this effective eye degradation. We feel that if such a relationship could be found, the analysis of complex noise problems will be simplified. However, we could find no such

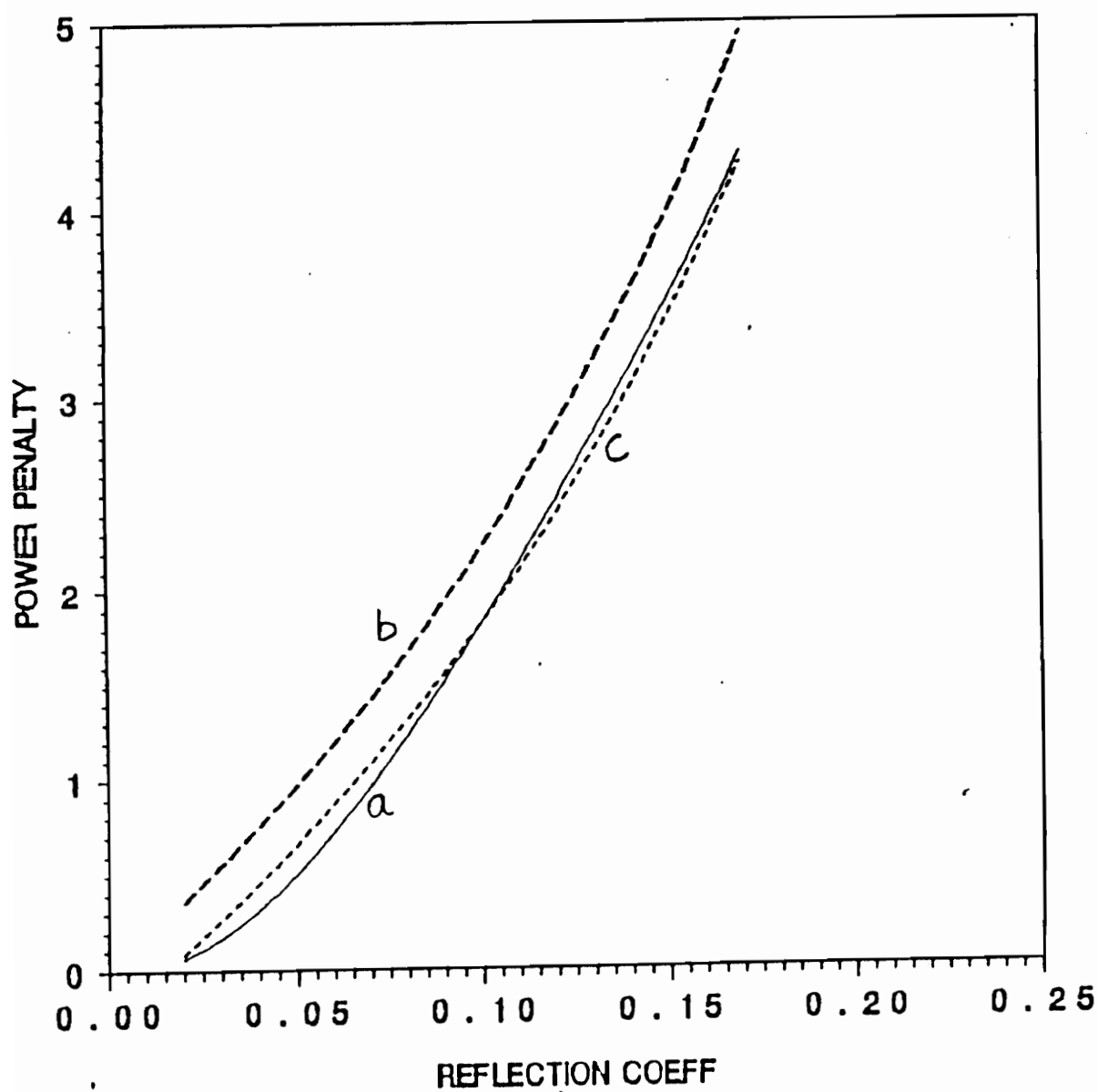


Fig. 3.4

Power penalties versus reflection coefficient R :

a) actual calculation

b) eye degradation approximation $\epsilon = \epsilon_{\max}$

c) eye degradation approximation $\epsilon = \epsilon_{\max} - 0.03$

obvious relationship. We think that the steepness of the distribution function at the ends is in some way responsible for this simple relationship between the reflection coefficient and the effective eye degradation.

It may be of interest, as a suggestion for future work, to determine whether the power degradations resulting from other ISI distributions can be similarly fit using an effective eye degradation.

3.5 Uniform approximation for pdf of RIN

The eye degradation approximation assumes that the pdf of the RIN is a delta function at the extreme. Although the eye degradation approximation is useful when the maximum RIN is much less than the signal, it is not useful when the value of the noise is comparable to the signal level. Hence there is a need to approximate the noise by other distributions. In this section, we approximate the RIN by a uniform distribution. We return to the formalism developed in section 3.1.

The function F is approximated by a straight line going through :

$$F \left\{ \frac{1}{2R} \left(1 - \frac{u_0}{\alpha} \right) \right\} = P_0 = \frac{1}{2} 10^{-9} \quad (3.5.1)$$

where α is the signal to thermal noise amplitude ratio, u is the normalized thermal noise variable, u_0 corresponds to that value of the normalized thermal noise which satisfies eq.(3.5.1) and $F(\cdot)$ is given by eq.(3.1.7). Since F is assumed to be an even function, $F(0) = 1/2$. This representation of F is plotted in Fig. (3.5). From the figure, it is evident that F reaches the value 1 at $2\alpha - u_0$. The equation for the straight line F is given by :

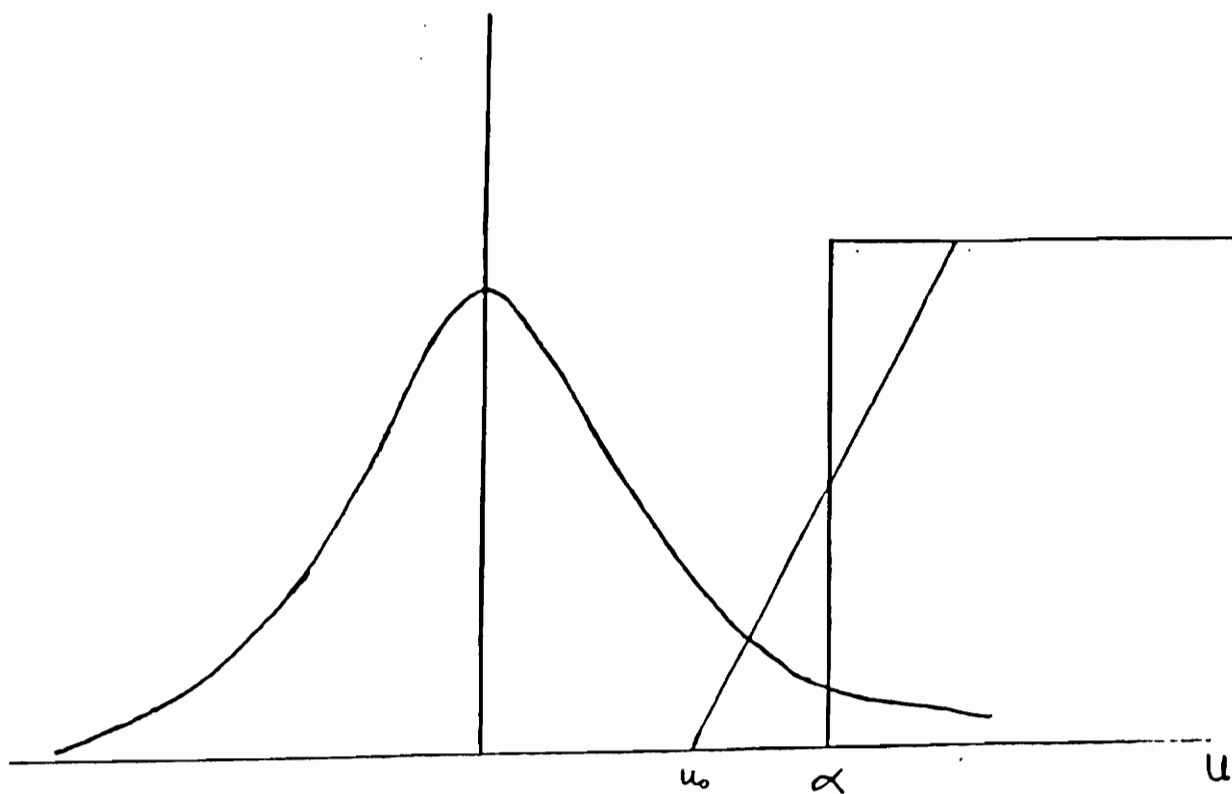


Fig. 3.5 Cumulative distribution function of RIN approximated as a straight line

$$F = \frac{u - u_0}{2(\alpha - u_0)} .$$

The probability of error is given by :

$$P_E = Q(2\alpha - u_0) + \frac{1}{\sqrt{2\pi}} \int_{u_0}^{2\alpha - u_0} du \exp\left(-\frac{u^2}{2}\right) \frac{(u - u_0)}{2(\alpha - u_0)} \quad (3.5.2)$$

The integral is evaluated as follows :

$$P_1 = \frac{1}{2(\alpha - u_0)} \left[\frac{1}{\sqrt{2\pi}} \exp\left(-\frac{u_0^2}{2}\right) - u_0 Q(u_0) - \frac{1}{\sqrt{2\pi}} \exp\left(-\frac{(2\alpha - u_0)^2}{2}\right) + (2\alpha - u_0) Q(2\alpha - u_0) \right] \quad (3.5.3)$$

But, for small P_E , u_0 is large, in which case,

$$\frac{1}{\sqrt{2\pi}} \exp\left(-\frac{u_0^2}{2}\right) - u_0 Q(u_0) \approx \frac{1}{\sqrt{2\pi}} \frac{\exp\left(-\frac{u_0^2}{2}\right)}{u_0^2} \quad (3.5.4)$$

Denoting the argument of F by κ , i.e.

$$\frac{1}{2R} \left(1 - \frac{u_0}{\alpha}\right) = \kappa$$

Then,

$$u_0 = \alpha(1 - \epsilon) ; \quad 2\alpha - u_0 = \alpha(1 + \epsilon) \quad (3.5.5)$$

where $\epsilon = 2R\kappa$.

Then,

$$\begin{aligned}
 P_1 &= \frac{1}{2\alpha^3\sqrt{2\pi}} \left[\frac{\exp(-\alpha^2(1-\epsilon)^2)}{(1-\epsilon)^2} - \frac{\exp(-\alpha^2(1+\epsilon)^2)}{(1+\epsilon)^2} \right] \\
 &= \frac{\exp(-\alpha^2\frac{(1+\epsilon^2)}{2})}{\sqrt{2\pi}\alpha^3\epsilon(1-\epsilon^2)^2} \left\{ (1+\epsilon^2)^2 \sinh \alpha^2\epsilon + 2\epsilon \cosh \alpha^2\epsilon \right\}
 \end{aligned} \tag{3.5.6}$$

As $\epsilon \rightarrow 0$,

$$P_1 \rightarrow \frac{\exp(-\frac{\alpha^2}{2})}{\sqrt{2\pi}\alpha^3\epsilon} \alpha^2\epsilon \approx Q(\alpha) \tag{3.5.7}$$

which is the result in the absence of reflections.

Setting $P_1 = 1/2 \cdot 10^{-9}$, and using equation (3.5.6), it is possible to compute power penalties as a function of ϵ . Once a value for κ has been fixed, the penalties can be computed directly as a function of R , since R and κ are simply related. κ is a parameter that is determined directly from the probability density function of the random variable x . F has been approximated as a straight line, which essentially means that the pdf of the noise has been approximated by a uniform distribution.

Now, $F_x(\kappa) = 1/2 \cdot 10^{-9}$ i.e. the probability that $x > \kappa = 0.5 \cdot 10^{-9}$. For all practical purposes then, x is a random variable that is uniformly distributed from $-\kappa$ to

+ κ . The parameter κ must be independently determined from the nature of the noise.

It is known that the interferometric noise is bounded at ± 2 (R has been decoupled from the noise in this formalism) and further, the variance of the interferometric noise = 2.

This suggests two different methods to fix a value of κ .

One way is to equate the bounds of the uniform approximation to the bounds of the actual distribution, i.e. $\kappa = 2$.

The other way is to choose κ such that the variances of the two distributions are equal. The variance of a uniform bounded distribution is easily calculated to be $\kappa^2 / 3$ from which κ is calculated to be equal to the square root of 6 which equals 2.449. Using these two values of κ , the power penalties are plotted in fig. (3.6) as a function of R , the reflection coefficient.

The graph shows that the value of κ corresponding to the matching bound results in power penalties that are very close to the actual results while the value of κ corresponding to matching the variance provides poorer results, but nevertheless better than the Gaussian approximation. This is probably a consequence of the steepness of the actual p.d.f and the fact that the errors are largely caused by the region near the extremity of the probability density function. Further, the approximation of the bounded p.d.f by other bounded p.d.fs provides better results than the Gaussian approximation with its infinite tail.

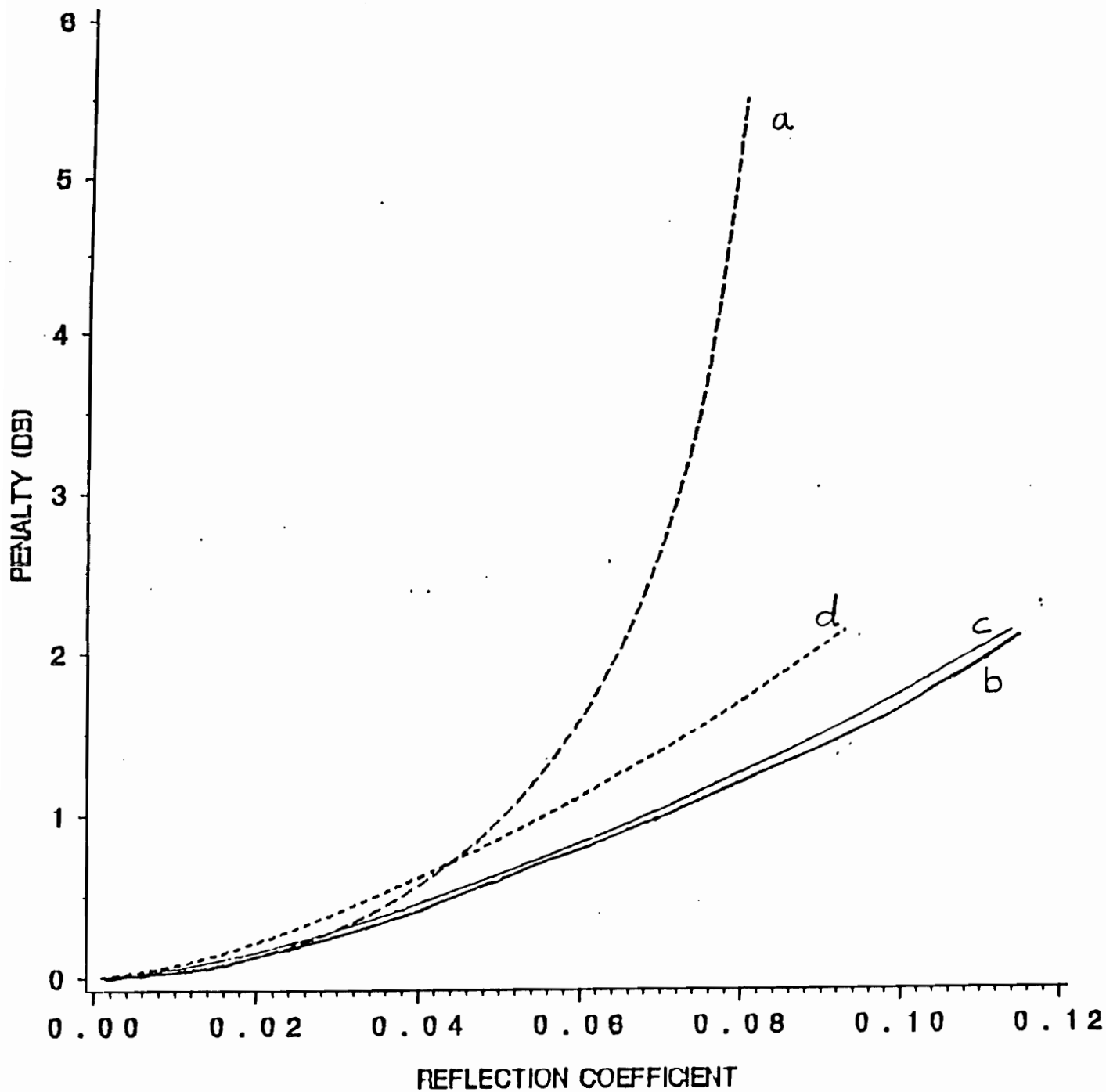


Fig. 3.6

Power penalties versus reflection coefficient R :

- a) Gaussian distribution**
- b) actual distribution**
- c) uniform distribution with matching bounds**
- d) uniform distribution with matching variance**

3.6 Quadratic approximation for the pdf

The straight line approximation may be considered as the first term in a polynomial approximation. We consider next a cubic approximation to F which corresponds to a quadratic approximation to the probability density function; i.e., the p.d.f is of the form

$$f_x(x) = a_0 + a_2 x^2 \quad (3.6.1)$$

Any approximation made has to satisfy the basic characteristic of the p.d.f of the interferometric noise - that the p.d.f is an even function (all the odd moments are zero). Hence, in the quadratic approximation, there is no first order term in x .

For any function to be a possible probability density function, it must have these two fundamental properties :

- i) area under the curve must equal unity, i.e.

$$\int_{-\infty}^{\infty} f_x(x) dx = 1$$

- ii) $f_x(x)$ must be non-negative everywhere :

$$f_x(x) \geq 0 \text{ for all } x \in (-\infty, \infty)$$

Any polynomial approximation for the pdf of the interferometric noise therefore must satisfy these two criteria. There is, obviously, more than one possible polynomial that meets all of the above requirements, which means that the coefficients a_0 and a_2 are not unique, but are a function of the conditions of the problem. We decided to impose the following conditions upon the quadratic approximation for the p.d.f :

- i) The bounds on the quadratic approximation are the same as those on the actual p.d.f, which equals ± 2 .
- ii) The variance of the two p.d.fs are the same.

Thus, with the quadratic approximation both these conditions may be satisfied simultaneously whereas with the uniform approximation only one of the conditions may be satisfied.

Using these conditions, the coefficients a_0 and a_2 are calculated to be :

$$a_0 = 3/32 ; a_2 = 15/128 .$$

The probability of error is then given by :

$$P_E = \frac{1}{\sqrt{2\pi}} \int_{-\infty}^{\infty} du \exp\left(-\frac{u^2}{2}\right) \int_{\frac{1}{2R}(1-\frac{u}{\alpha})}^2 dx \left(\frac{3}{32} + \frac{15}{128}x^2\right) \quad (3.6.2)$$

$$= \frac{1}{\sqrt{2\pi}} \int_{-\infty}^{\infty} du \exp\left(-\frac{u^2}{2}\right) \left\{ 0.5 - \frac{3}{64R}\left(1 - \frac{u}{\alpha}\right) - \frac{15}{1024R^3}\left(1 - \frac{u}{\alpha}\right)^3 \right\}$$

The power penalty is numerically obtained from this expression and is plotted in fig. (3.7). It is seen from figures (3.6) and (3.7) that the penalty obtained with this approximation provides a very good estimate to the actual penalty. There is not a significant difference between using this approximation and the uniform approximation with the same bounds. In the case of this specific distribution, owing to the steepness of the p.d.f, we think that any pdf that has the same bounds will provide a fairly good estimate of the power penalty. In general, however, we anticipate that a quadratic p.d.f will provide a better approximation over a wider class of distributions than the uniform distribution will.

It must be reemphasized at this point that there is more than one possible quadratic approximation for the pdf. The coefficients a_0 and a_2 can also be obtained by setting higher order moments equal. For example, in this case, a_0 and a_2 could have been obtained by

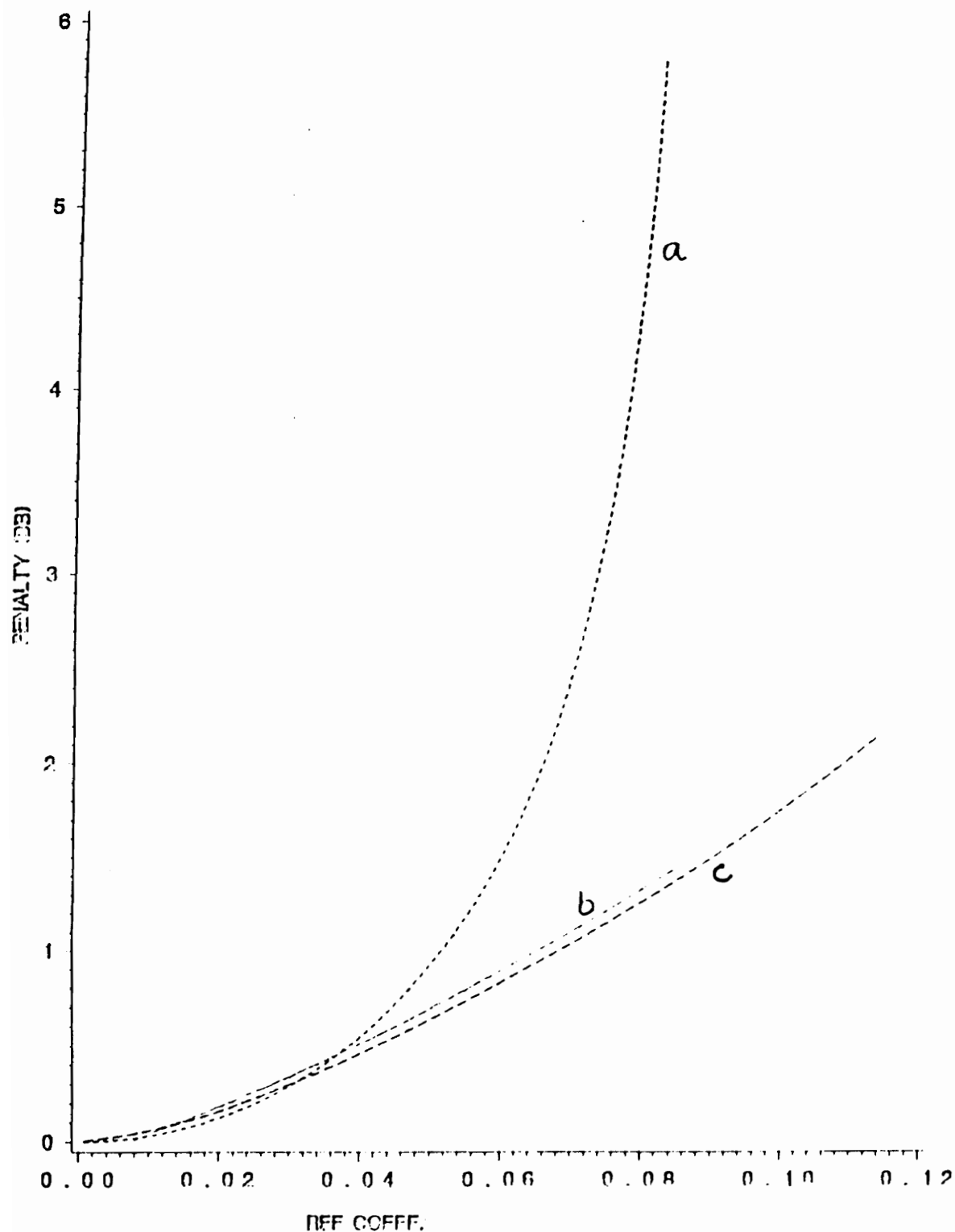


Fig. 3.7 Power penalties versus reflection coefficient R :
 a) Gaussian distribution
 b) uniform distribution with matching bound
 c) quadratic distribution

setting the second and fourth order moments equal and letting the bounds of the distribution be different. However, for bounded distributions, the bounds play an important role in determining the error probability, and it is more useful to approximate bounded distributions by other distributions having the same bounds.

In this chapter, the impact of RIN on system performance has been explained. We have made a number of approximations for the p.d.f of RIN. Power penalties have been computed with each of these approximations. We see that the results from these approximations match those with the exact calculations fairly well. In fact, one of the key results of this thesis is that when the p.d.f of a noise process is a bounded one, other simple bounded p.d.fs, and even an eye degradation, are very good approximations. A natural question is how good these approximate methods are for non-bounded distributions. It is shown in Appendix B that these approximations are not applicable in all situations. We show there that the quadratic approximation, which is bounded, is not useful in describing an exponential distribution, which has a tail extending to infinity.

The analysis in this chapter has been done under several simplifying assumptions. Key among them are the assumptions that RIN and thermal noise are the only sources of degradations and that there is only pair of reflection points in the system. In practice, neither of these conditions is likely to be satisfied. In the next chapter, some of these restrictions are lifted.

4.0 Extensions of the model

In chapters two and three, the basic theory explaining the phenomenon of RIN and its impact on system performance was presented. The analysis was made with two major assumptions which are reiterated here :

- i) the reflectivities at the discontinuities are small, as a result of which higher order terms in the reflection coefficient, corresponding to multiple passes, are neglected.
- ii) RIN is the only impairment in the system, besides the receiver thermal noise, of course.

Further, for simplicity, only one pair of reflectors was assumed to be present in the system. However, in practice, in any fiber system, there are more than two refractive index discontinuities, i.e. there are more than two reflectors in the system. Also, typically there are other impairments in the system. Sodhi [13] has shown that power penalties are not additive. Further, even though the reflectivities have been assumed to be small, there actually exist multiple reflections at any pair of reflectors. While these added reflections have a small impact on noise power, they have a significant impact on the tails of the distribution, and as mentioned previously, it is the tails that have the greatest impact on the error probability and the power penalty. Hence, there is a need to relax the assumptions

made in the previous chapters and to generalize the theory to take into account all of these factors.

Another reason for investigating these other effects is that there exist some discrepancies between the experimental results and the theoretical predictions for the power penalties (Fig. (2.2), [6]). Some of these phenomena, individually or in concert, may explain these discrepancies.

In the following sections, each of these factors is considered individually and its impact on system performance assessed. In section 4.1, we assume a finite extinction ratio as a typical impairment present in a fiber system. Section 4.2 deals with multiple reflections at a single pair of reflectors, while the effect of a multiplicity of reflection points is considered in section 4.3.

4.1 Combined effect of an extinction ratio and RIN

In an OOK system, ideally, there is no optical power output from the laser when a “zero” is transmitted. However, with aging etc. the laser does not completely shut off when a zero is to be transmitted. It transmits a small but finite fraction of the power outputted when a one is transmitted. The ratio of the power transmitted during a “one” to that during a zero is called the extinction ratio, which is designated as $1/\epsilon$, so that large extinction ratios correspond to small values of ϵ .

In the presence of an extinction ratio $1/\epsilon$, the electrical current at the receiver is given by (eq.(3.1.2)) :

$$i(t) = E_0^2 \{ a(t) + v(t) \} + n(t) \quad (4.1.1a)$$

when a “one” is transmitted and

$$i(t) = E_0^2 \{ \epsilon a(t) + \epsilon v(t) \} + n(t) \quad (4.1.1b)$$

when a zero is transmitted, instead of $i(t)$ equaling only the thermal noise when a zero is transmitted. Here, $v(t)$ is the interferometric noise term given by eq.(3.1.3) :

$$v(t) = 2\sqrt{a(t).a(t - \tau)} R \cos (\omega_0 \tau + \Phi(t, \tau))$$

The symbols in all these equations are as defined in chapter 3.

To simplify the analysis, a Gaussian distribution is assumed for RIN. As discussed in chapter 3, this is generally a conservative assumption.

The means and the variances μ_1 , μ_0 , σ_1^2 , σ_0^2 of $i(t)$ are calculated to be, following procedures similar to those in section 3.2 :

$$\begin{aligned} \mu_1 &= E_0^2, \quad \mu_0 = \epsilon \mu_1 ; \\ \sigma_1^2 &= \langle I^2 \rangle - \langle I \rangle^2 = \sigma_n^2 + \mu_1^2 R^2; \quad \sigma_0^2 = \sigma_n^2 + \mu_0^2 R^2; \end{aligned} \quad (4.1.2)$$

where σ_n^2 is the variance of the receiver thermal noise.

In this case, the receiver decision threshold D is no longer the same i.e. it is no longer at $\mu_1/2$. Because the finite extinction ratio is a phenomenon that, while being a degradation, is not random in nature - the degradation is fixed and deterministic (it may change slowly with time). Hence, the effects are sought to be minimized by reoptimizing the decision threshold. Now, the probability of error is given by (eq.(3.2.3)) :

$$P_E = \frac{1}{2} Q\left(\frac{\mu_1 - D}{\sigma_1}\right) + \frac{1}{2} Q\left(\frac{D - \mu_0}{\sigma_0}\right)$$

It may be shown [12] that the error probability is very nearly minimized when there is an equal probability of “zero” and “one” errors occurring, which then gives :

$$\frac{\mu_1 - D}{\sigma_1} = \frac{D - \mu_0}{\sigma_0} = k_1 \quad (4.1.3)$$

where k_1 is the argument of the Q function. Using eq.(4.1.2),

$$\frac{\mu_1 - D}{\sqrt{\sigma_n^2 + \mu_1^2 R^2}} = \frac{D - \mu_0}{\sqrt{\sigma_n^2 + \epsilon^2 \mu_1^2 R^2}} = k_1 \quad (4.1.4)$$

or,

$$\frac{\mu_1 (1 - \epsilon)}{\sqrt{\sigma_n^2 + \mu_1^2 R^2} + \sqrt{\sigma_n^2 + \epsilon^2 \mu_1^2 R^2}} = k_1 \quad (4.1.5)$$

Letting $1 - \epsilon = b$, and after some algebra ,

$$\mu_1 = \frac{2 \sigma_n b / k_1}{\left\{ \left[\left(\frac{b}{k_1} \right)^2 - R^2 (1 + \epsilon^2) \right]^2 - 4 R^4 \epsilon^2 \right\}^{1/2}} \quad (4.1.6)$$

For $\epsilon = 0$ and $R = 0$ (i.e. in the absence of RIN and extinction ratio), $\mu_1' = 2 \sigma_n k_1$.

Then, to maintain the same error probability, i.e. the same k_1 , the power penalty P is given by :

$$\begin{aligned}
P &= 10 \log \frac{\mu_1}{\mu'_1} \\
&= 10 \log \frac{b}{k_1^2 \left\{ \left[\left(\frac{b}{k_1} \right)^2 - R^2 (1 + \epsilon^2) \right]^2 - R^4 \epsilon^2 \right\}^{1/2}}
\end{aligned} \tag{4.1.7}$$

To maintain a 10^{-9} error probability, $k_1 = 6.0$. Then, the power penalty as a function of ϵ and R is given by :

$$P(\epsilon, R) = 10 \log \frac{b}{36 \left\{ \left[\left(\frac{b}{6} \right)^2 - R^2 (1 + \epsilon^2) \right]^2 - R^4 \epsilon^2 \right\}^{1/2}} \tag{4.1.8}$$

Note that for $\epsilon = 0$ this reduces to eq. (3.2.15). The differential power penalty, given by $P(\epsilon, R) - P(\epsilon, 0)$, where $P(\epsilon, R)$ is given by eq.(4.1.8), is plotted as a function of R in Fig. (4.1) for different values of ϵ . The curves indicate that there is an additional power penalty due to the extinction ratio which increases rapidly with R . The graphs also indicate that the maximum allowed R for a BER floor decreases with increasing ϵ ; for example,

$$R_{\max} = 0.16 \text{ for } \epsilon = 0, \text{ and } R_{\max} = 0.11 \text{ for } \epsilon = 0.2.$$

As indicated in the previous chapter, an alternative to treating the RIN as Gaussian distributed is to use an eye degradation approximation. In this case, if ϵ is the equivalent eye-degradation resulting from RIN, and ϵ_1 is the degradation associated with finite extinction ratio, then the total power penalty is given by :

$$P = -10 \log (1 - 2(\epsilon + \epsilon_1)) = -10 \log (1 - 4R - 2\epsilon_1) \tag{4.1.9}$$

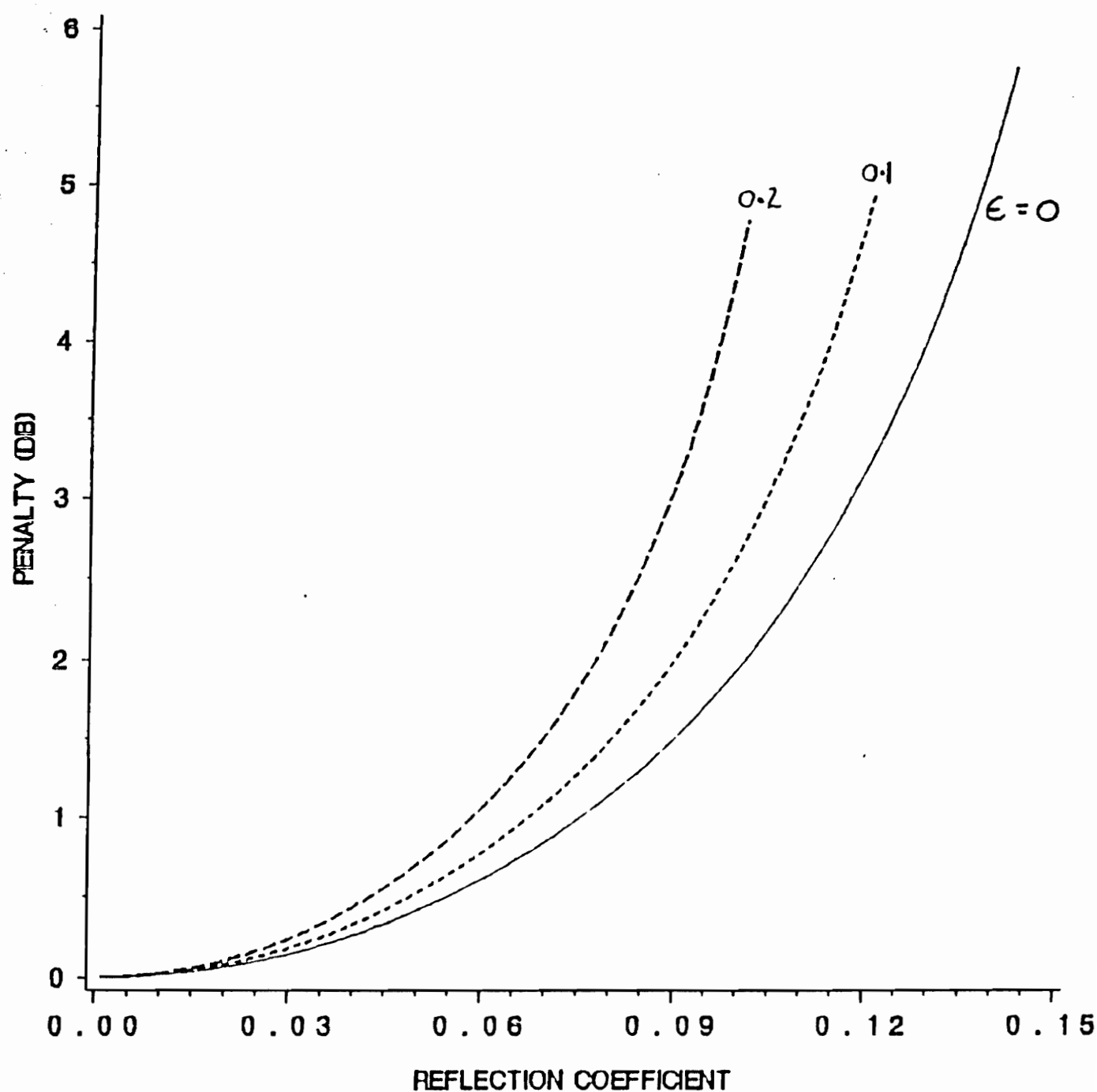


Fig. 4.1 Power penalty vs. reflection coefficient R for different values of extinction ratio $1 / \epsilon$

Hence, the incremental power penalty due to the additional degradation is given by :

$$P = -10 \log (1 - 4R - 2\varepsilon_1) + 10 \log (1 - 4R) \quad (4.1.10)$$

With the Gaussian approximation, the incremental power penalty due to the additional degradation is given by $P(\varepsilon, R) - P(0, R)$ where $p(\varepsilon, R)$ is given by eq.(4.1.8). This and eq.(4.1.10) are plotted in fig.(4.2). Examination of this plot indicates that for the range of parameters considered, the effect of additional degradations is less under the eye degradation approximation than it is under the Gaussian approximation. However, in both cases the penalty caused by reflections is greater when there are other impairments present in the system. This is at least qualitatively consistent with the measurements of Gimlett and Cheung [6]. Thus, other degradations, as given by the parameter ε_1 , may be a partial cause of the experimental degradations being larger than calculated by the previous theories.

4.2 Effect of multiple reflections

All of the prior analysis assume that the reflection induced noise is a result of a double reflection as shown in fig. (2.1). However, in reality, there are multiple reflections. As stated before, while the effects of these multiple reflections on noise power may be very small, it is not immediately obvious that the power penalties are also equally insensitive to this effect. In fact, this effect may be the more fundamental cause of the discrepancy between the theoretical and experimental results of Gimlett and Cheung [6]. There is, hence, some interest in seeing whether considering the effect of multiple reflections helps in resolving these discrepancies in the published results. In this section, an outline of the analysis of the effect of multiple reflections is presented. In a bid to keep the analysis simple, we have assumed that all other impairments in the system are absent.

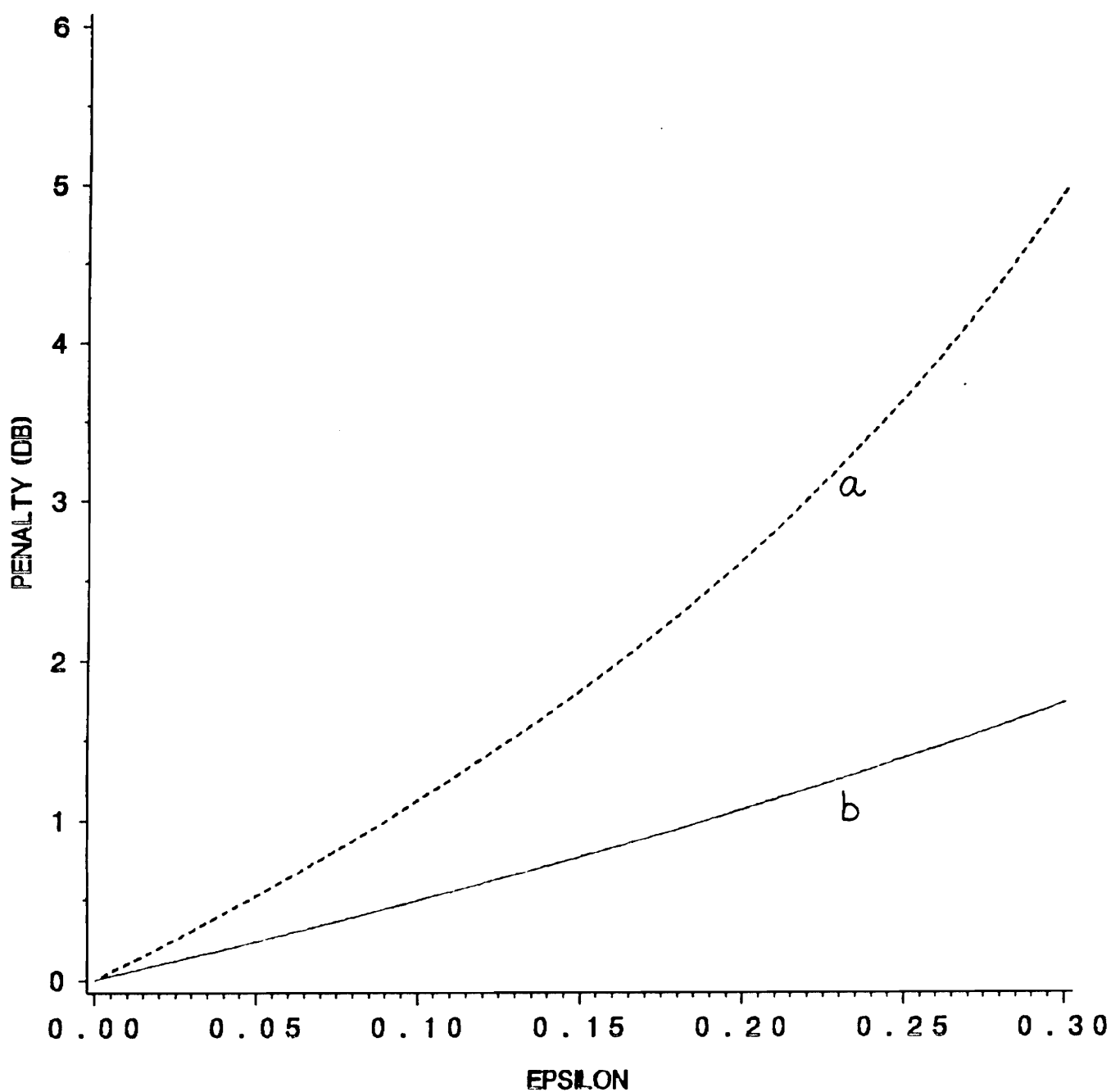


Fig. 4.2 Power penalty as a function of ϵ for $R = 0.03$
 a) Gaussian distribution for RIN
 b) eye-degradation approximation for RIN

We have shown in section 3.2 that the power penalty for RIN is easily calculated to be :

$$P = -5 \log (1 - 144 R^2)$$

under the assumptions that the pdf of RIN is Gaussian and that higher order terms of R are negligibly small. Just to see how good that approximation is, a next higher order term is considered :

$$v(t) = 2 \sqrt{a(t) a(t - \tau)} R \cos (\omega_0 \tau + \Phi(t, \tau)) + R^2 a(t - \tau) \quad (4.2.1)$$

where $v(t)$ is the expression for the interferometric noise. Then, the power penalty is found to be :

$$P = -5 \log (1 - 144(R^2 + R^4 / 4))$$

For all values of R of interest, the difference between these two power penalties is indeed negligibly small.

We have seen, however, (section 3.4) that for bounded interference the eye degradation approximation gives better results (compared to the exact calculation for two reflectors) than the Gaussian approximation. Consequently, we next consider the effect of multiple reflections approximated as an eye degradation. Initially only two pairs of reflections are considered. The electric field at the output of the interferometer is then given by :

$$e(t) = e_i(t) + R e_i(t - \tau) + R^2 e_i(t - 2\tau)$$

where $e_i(t)$ is the input field given by eq.(2.1.1). The intensity is given by :

$$\begin{aligned} i(t) &= |e(t)|^2 \\ &= e_i^2(t) + R^2 e_i^2(t - \tau) + R^4 e_i^2(t - 2\tau) + 2R e_i(t) e_i(t - \tau) + 2R^2 e_i(t) e_i(t - 2\tau) \\ &\quad + 2R^3 e_i(t - \tau) e_i(t - 2\tau) \end{aligned} \quad (4.2.1)$$

Neglecting terms of degree higher than R^2 , we have :

$$i(t) = e_i^2(t) + 2R e_i(t) e_i(t - \tau) + R^2 e_i^2(t - \tau) + 2R^2 e_i(t) e_i(t - 2\tau) \quad (4.2.2)$$

The last three terms describe the interference terms. In the incoherent regime, these terms are essentially uncorrelated. The peak magnitude of the degradation, relative to the signal, is bounded by $2R + 3R^2$. Setting this equal to the maximum eye degradation gives :

$$\epsilon = 2R + 3R^2 \quad (4.2.3)$$

The power penalty P is then given by, according to eq.(3.4.3),

$$\begin{aligned} P &= -10 \log(1 - 2\epsilon) \\ &= -10 \log(1 - 2(2R + 3R^2)) \end{aligned} \quad (4.2.4)$$

Similarly, considering the effects of three pairs of reflections, neglecting terms of degree R^4 and higher, the multiple reflections are estimated by an eye degradation given by :

$$\epsilon = 2R + 3R^2 + 4R^3 \quad (4.2.5)$$

In the general case then, with an infinite number of reflections,

$$\epsilon = 2R + 3R^2 + 4R^3 + \dots + mR^{m+1} + \dots \quad (4.2.6)$$

This is easily evaluated to give an effective eye degradation described by :

$$\epsilon_{\text{eff}} = R(2 - R) / (1 - R)^2 \quad (4.2.7)$$

The power penalty is then given by :

$$P = -10 \log(1 - 2\epsilon_{\text{eff}})$$

$$= -10 \log \{ 1 - 2R (2 - R) / (1 - R)^2 \} \quad (4.2.8)$$

The effect of multiple reflections on power penalty is compared with that of a double reflection, with both being approximated as eye degradations, by plotting eq.(4.2.8) and (3.4.3) in fig. (4.3). It is seen that the effect of multiple reflections is fairly significant for not-too-small values of R . It follows from equations (3.4.3) and (4.2.8) that the effect of multiple reflections (using the eye degradation approximation) is to result in an effective reflection coefficient given by :

$$R_{\text{eff}} = \epsilon_{\text{eff}} / 2 = R (2 - R) / 2 (1 - R)^2 \quad (4.2.9)$$

For very small values of R , $R_{\text{eff}} = R$. But as R increases, there is a slight difference between R_{eff} and R .

In this section, we have shown that while making a Gaussian approximation for the probability density function of RIN, the effect of multiple reflections is negligibly small. However, while making an eye degradation approximation, the effects are not that small. For reasons mentioned earlier, we feel that an eye degradation approximation is a more reasonable one to make in this situation. Hence, multiple reflection effects may indeed be one cause, among many, which explains the discrepancies between theory and experiment.

4.3 Effect of a multiplicity of reflection points

The analysis of RIN presented thus far is logically extended to consider, instead of just two, a multiplicity of reflectors in any fiber system. In this section, we consider the effect of three and four reflectors in the system. Gimlett and Cheung [6] have considered this effect. However, they made a simple Gaussian approximation for the probability

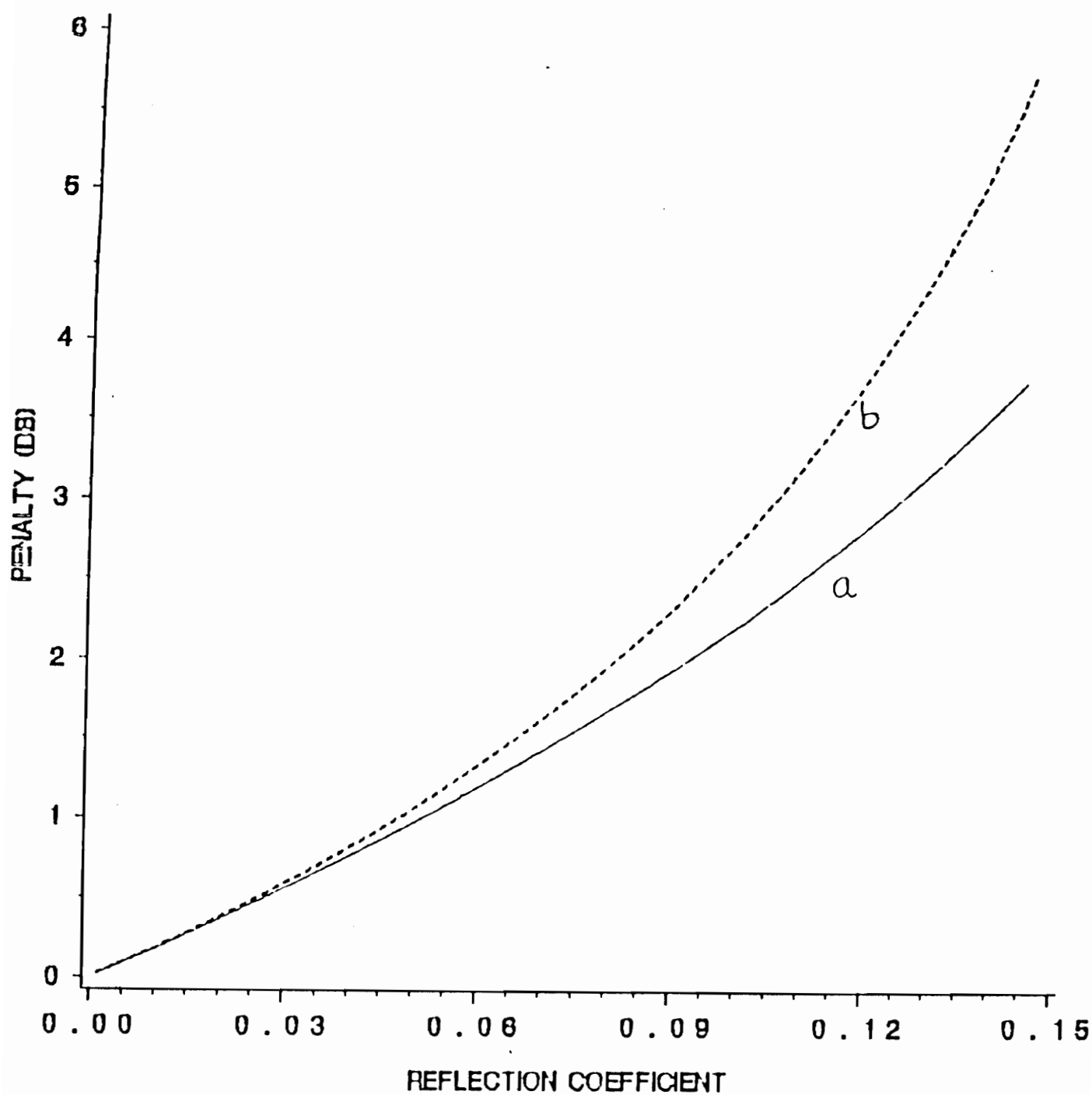


Fig. 4.3 Power penalty vs. reflection coefficient R with RIN being approximated as an eye degradation :
 a) single pair of reflections
 b) multiple reflections

density function of RIN. The pdf of RIN is indeed Gaussian when the number of reflectors is large. However, for a smaller number of reflection points, the pdf is not Gaussian. For this case of a few reflection points (typically three or four), we have attempted to approximate the pdf by a uniform distribution and a quadratic distribution, following the techniques developed in chapter 3. Further, we have also approximated the actual probability density function of RIN by using a Gram Charlier series approximation. The Gaussian approximation has also been used and these various approximations are compared to one another.

A fiber transmission line having N refractive index discontinuities (i.e. N reflectors) is considered. The resultant electric field at the output of the last reflector is given by :

$$\begin{aligned} e_{out}(t) = & e_{in}(t) + \sqrt{R_{21}} e_{in}(t - \tau_{21}) + \sqrt{R_{31}} e_{in}(t - \tau_{31}) \\ & + \sqrt{R_{32}} e_{in}(t - \tau_{32}) \dots + \sqrt{R_{ij}} e_{in}(t - \tau_{ij}) + \dots \end{aligned} \quad (4.3.1)$$

where only double reflections are considered. Here, τ_{ij} is the round trip delay time for the i^{th} and j^{th} discontinuities, and R_{ij} is a generalized reflection coefficient defined by $R_{ij} = \beta_{ij} (R_i R_j)^{0.5}$ where β_{ij} is the transmittance between the two discontinuities. Once again, polarisation effects have been neglected and for simplicity, so have the losses, i.e. $\beta_{ij} = 1$ for all i and j . The input field e_{in} is described by eq. (2.1.1). The light intensity detected at the receiver is then given by, as a simple extension of eq.(2.1.3) :

$$i(t) = E_0^2(t) \left\{ 1 + 2 \sum_{i=2}^N \sum_{j=1}^{i-1} R_{ij} \cos(\omega_0 \tau_{ij} + \Phi(t, \tau_{ij})) \right\} \quad (4.3.3)$$

The variable $\Phi(t, \tau_{ij})$ is essentially a phase difference given by :

$$\Phi(t, \tau_{ij}) = \varphi(t) - \varphi(t - \tau_{ij})$$

As was done in chapter 2, we assume that the interference is incoherent - the situation most commonly encountered in practice. When $2\pi\Delta\nu \tau_{ij} \gg 1$ and $2\pi\Delta\nu |\tau_{ij} - \tau_{kl}| \gg 1$ (where $\Delta\nu$ is the laser linewidth), $i \neq k, j \neq l$, all terms combine incoherently. Following the analysis in section 3.2, the power spectral density for RIN in this case (i.e multiplicity of reflection points with incoherent interference) is expressed as :

$$RIN(f) \approx \frac{4}{\pi} \left[\frac{\Delta\vartheta}{f^2 + (\Delta\vartheta)^2} \right] \sum_{i=2}^N \sum_{j=1}^{i-1} R_{ij}^2 \quad (4.3.4)$$

This expression indicates that the magnitude of the RIN increases rapidly with the number of discontinuities.

Next, the effect of a multiplicity of reflectors on system penalties is considered. As in chapter 3, a binary on-off keying scheme with NRZ formatted data is considered. The laser pulse wave form is given by eq.(3.1.1) :

$$\begin{aligned} a(t) &= 1, & 0 < t < T \\ &= 0, & \text{otherwise} \end{aligned} \quad (4.3.5)$$

where T is the bit duration. Again, following the formalism developed in chapter 3, the signal at the receiver decision point is of the form :

$$y = a + xRa + n$$

The conditions and the assumptions made in chapter 3 still hold here i.e. the noise is asymmetric and so the errors are dominated by those in the "one" state, but the receiver decision threshold is still the same. The error probability can then be expressed by equations (3.1.5) and (3.1.6). For convenience, eq.(3.1.6) is repeated here :

$$P_E = \frac{1}{\sqrt{2\pi}} \int_{-\infty}^{\infty} du \exp(-\frac{u^2}{2}) F \left\{ \frac{1}{2aR} \left(1 - \frac{u}{\alpha} \right) \right\} \quad (3.1.6)$$

where all the terms have the same meaning. Hence,

$$F(\xi) = \int_{\xi}^{\infty} dx p(x) = \text{prob. } (x > \xi) \quad (4.3.6)$$

as in chapter 3. Once again, as in chapter 3, we make different approximations for the probability density function of the random variable x which represents the interferometric noise due to a multiplicity of reflectors. For the case of a single pair of reflectors, the variable x was given by :

$$x = 2 \cos (\omega_0 \tau + \Phi(t, \tau)) \quad (4.3.7)$$

In the case of N reflectors there are $N(N-1)/2$ interferometric terms which are given by :

$$x = 2 \cos (\omega_0 \tau_{21} + \Phi(t, \tau_{21})) + 2 \cos (\omega_0 \tau_{31} + \Phi(t, \tau_{31})) + \dots + 2 \cos (\omega_0 \tau_{ij} + \Phi(t, \tau_{ij})) + \dots \quad (4.3.7)$$

where τ_{ij} has the same meaning mentioned earlier. The analysis is first done with a Gaussian approximation for the probability density function of RIN.

In the Gaussian case, which Gimlett and Cheung [6] have considered, the power penalties are obtained by simply extending the result given in eq.(3.2.14) to account for the

many terms :

$$P = -5 \log \left[1 - 144 \sum_{i=2}^N \sum_{j=1}^{i-1} R_{ij}^2 \right] \quad (4.3.8)$$

We have assumed that polarization effects are negligible. However, in a multiple reflector situation, that may not always be true. For randomly aligned polarizations, the average value of $R_{ij}^2 = 0.5 \beta^2 (R_i R_j)$. In that case, the power penalty is reduced by a factor of two. Again, in a multiple reflector situation, the transmittance β may not $= 1$ i.e. there may be some losses, in which case the power penalty reduces further. Eq.(4.3.8) is plotted in fig.(4.4) [6]. Examination of the figure shows that the power penalty increases rapidly with the number of reflectors. Also shown in the figure is a curve considering a 0.5 dB loss between adjacent reflection points (curve c). It is seen that even for reflections as small as 1 %, significant penalties or BER floors occur if many such reflections are present in the fiber path. The presence of losses, however, helps to reduce the adverse impact of multiple reflection points.

As mentioned earlier, the pdf of RIN tends to Gaussian if a large number of reflection points are present. However, if the number of reflectors are small, for example three or four, the pdf is not Gaussian. In that regime, the pdf has to be estimated. We adopt the techniques of chapter 3 here and approximate the probability density function with a uniform and a quadratic approximation. We discuss first the uniform approximation.

As in section 3.5, we approximate the pdf by a random variable uniformly distributed from $-\kappa$ to $+\kappa$. The analysis is identical to that in section 3.5. The only question is how to determine the bounds of the distribution. Once again, the choice for κ is such that it satisfies one of the following two conditions :

- a) the bounds of the two distribution are the same
- b) the variance of the two distributions is the same.

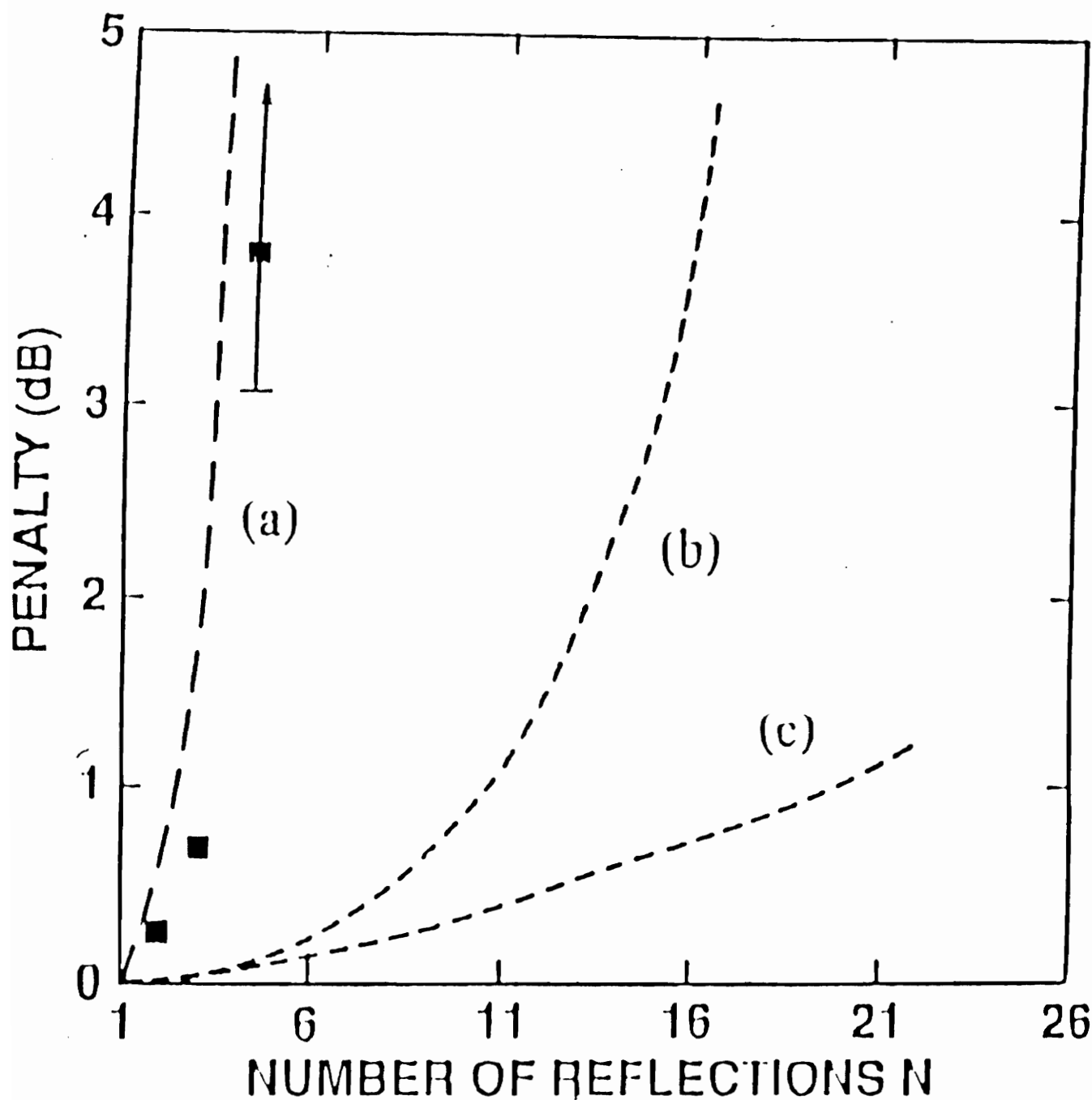


Fig. 4.4 Power penalty vs. number of reflectors for different values of reflection coefficient R :
a) $R = 0.06$
b) $R = 0.01$
c) $R = 0.01$ and 0.5 dB loss between adjacent reflection points
(taken from ref.[6] The \blacksquare represent experimental measurement)

It is to be noted that both these conditions cannot be satisfied simultaneously by a random variable which is uniformly distributed. The 3-reflector situation is first considered. In this case, there are 3 reflection terms. Using the formalism developed in section 3.5, each random variable is bounded at ± 2 . Hence, the random variable that is the sum of these three extends from -6 to + 6. As will be shown later, the variance of this random variable is 6. Matching the bounds of the two distributions results in $\kappa = 6$. Using eq.(3.5.6), the power penalty is computed as a function of R. The power penalty with the Gaussian approximation is computed too, for comparison. It is seen that the uniform approximation with the matching bound gives poorer results than even the Gaussian approximation. Evidently, bound matching, which was so effective in the two-reflector situation, is no longer a good approximation. This is true for the four- reflector case too. Thus it seems that the pdf of the distribution is no longer as steep at the ends as it was in the two reflector case.

Consider the 3-reflector case again, assuming now that the variances are matched rather than the bounds. The variance of a random variable uniformly distributed from $-\kappa$ to $+\kappa$ is given by $\kappa^2/3$. Equating that to 6, which is the variance of this distribution, gives

$$\frac{\kappa^2}{3} = 6 \Rightarrow \kappa = \sqrt{18} = 4.2426$$

The power penalty is plotted as a function of R, using this value of κ , in fig. (4.5). The penalty with the Gaussian approximation is also plotted in the same figure. The uniform approximation gives a lower penalty as compared to the Gaussian, except for very small values of R.

For the four-reflector situation, the variance is 12. Hence, $\kappa = 6$. The penalty is plotted as a function of R in fig.(4.6). The corresponding Gaussian case is plotted too. Once again, the uniform approximation provides a lower power penalty except at very small values of R.

The reason that the variance matching technique is providing better results seems to

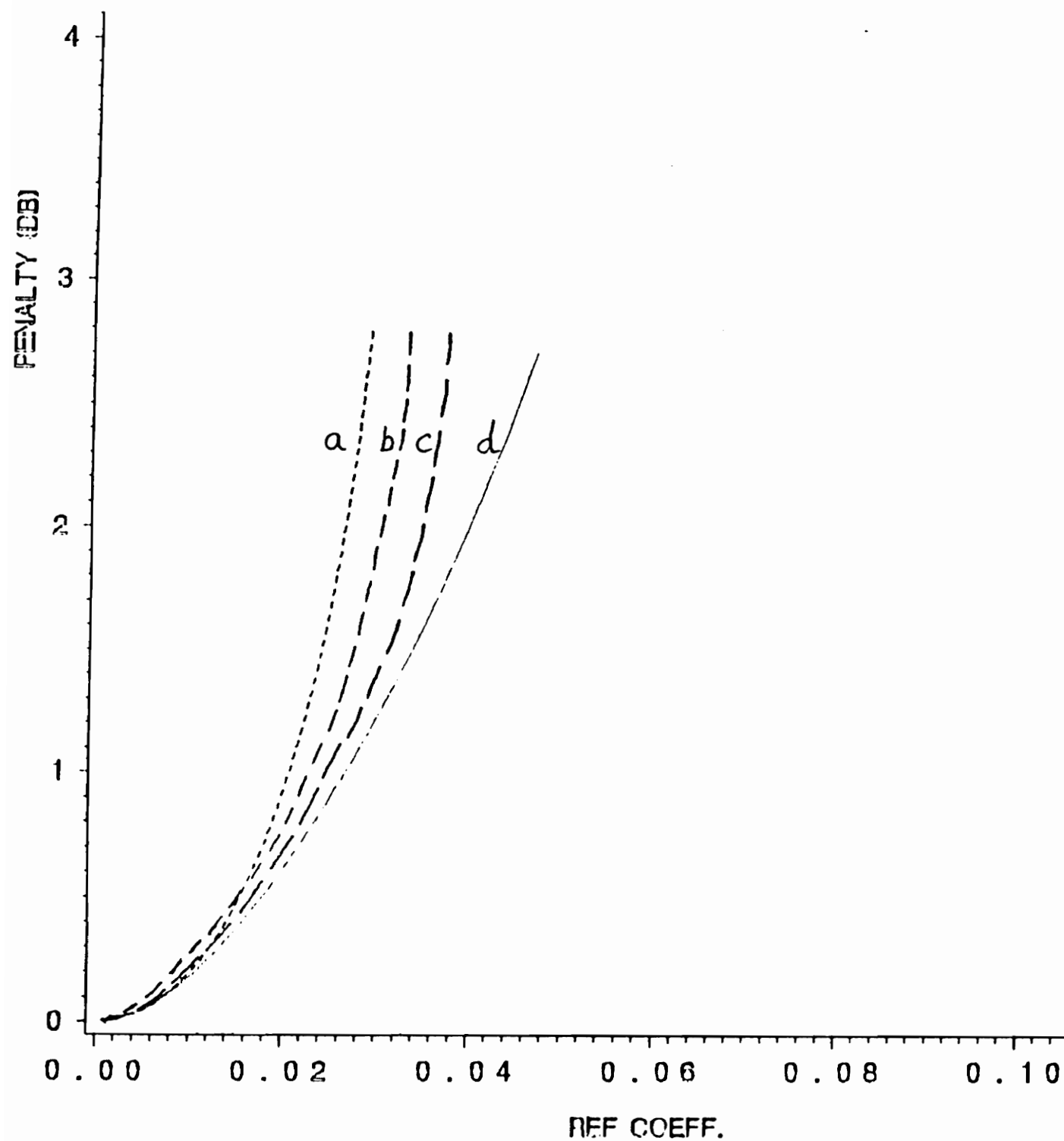


Fig. 4.5

Power penalty vs. reflection coefficient R for 3 reflectors and different approximations for the pdf of RIN:

- a) Gaussian approximation
- b) uniform approximation
- c) quadratic approximation
- d) Gram-Charlier series expansion

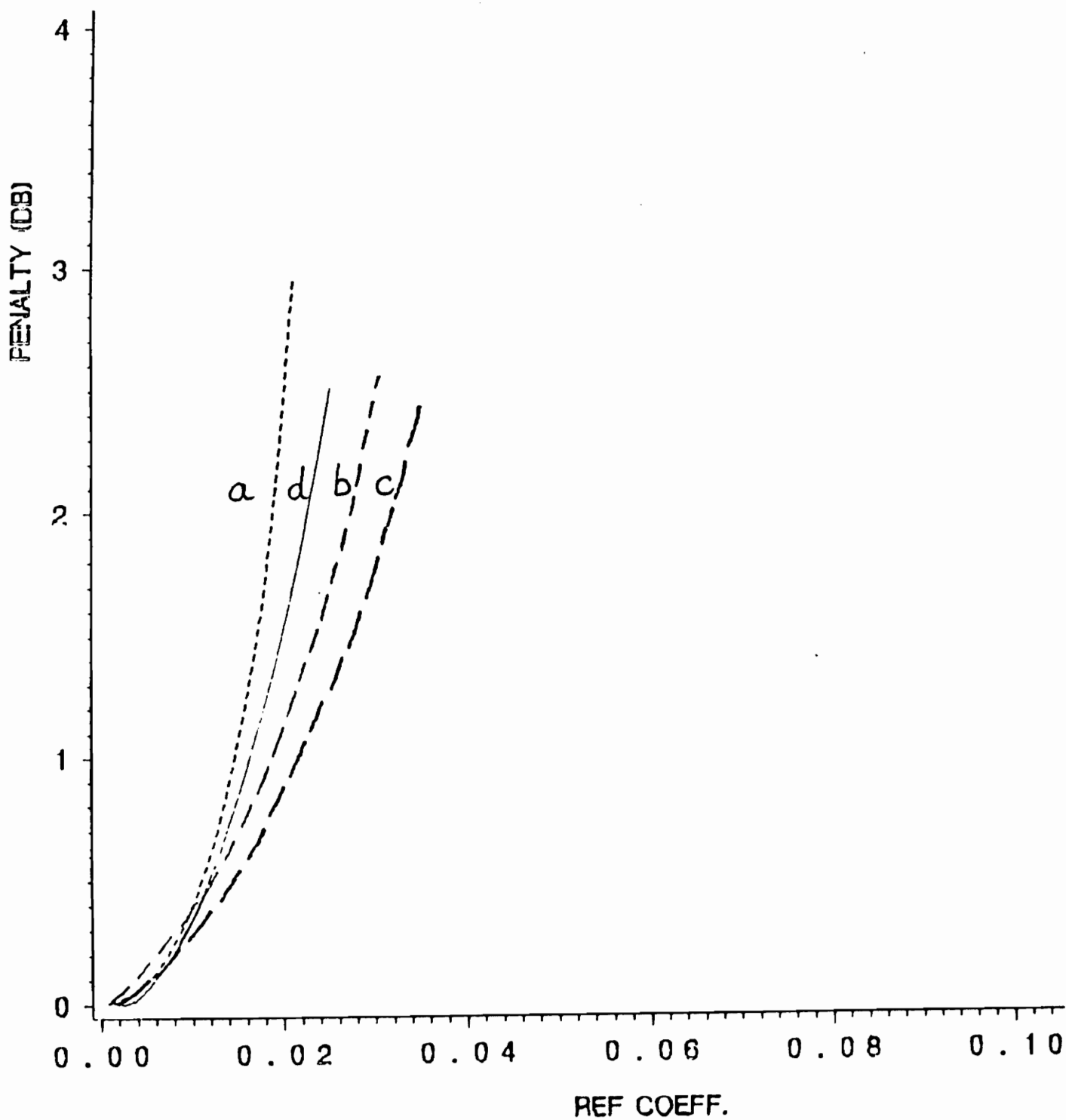


Fig. 4.6 Power penalty versus reflection coefficient for 4 reflectors
 a) Gaussian approximation
 b) uniform approximation
 c) quadratic approximation
 d) Gram-Charlier series expansion

lie in the fact that the probability density function of the interferometric noise is no longer as steep as it was in the two-reflector situation. This is just stated now, but will be demonstrated later in this section.

Having approximated the pdf by a uniform random variable, there is some interest in using the quadratic approximation of section 3.6 to see if that provides better results. In this case, however, just equating the bounds and the variances does not work because the pdf is not non-negative throughout. Hence, an additional constraint is imposed. The quadratic expression representing the pdf is assumed to go to zero at the boundaries. Imposing this condition, however, it is not possible to find a quadratic expression that has both the bounds and the variance equal to those of the actual pdf. We decided that matching the variance is more important in this case. The pdf is then assumed to be of the form, as in section 3.6,

$$f_x(x) = a_0 + a_2 x^2 \quad (4.3.9)$$

defined from $-\kappa$ to $+\kappa$, which are unknown just now. Using the condition that the pdf goes to zero at the extremes,

$$a_0 + \kappa^2 a_2 = 0 \Rightarrow a_0 = -\kappa^2 a_2$$

This condition combined with the other two conditions that the area under the curve equals unity and that the variances are the same enables us to determine the coefficients a_0 and a_2 and the bound κ . For the 3-reflector case, $f_x(x)$ is then found to be :

$$f_x(x) = 0.1369 - 4.56 (10)^{-3} x^2 \quad (4.3.10)$$

with the bound $\kappa = 5.477$.

For the 4-reflector case, the pdf is found to be :

$$f_x(x) = 0.0968 - 1.613 (10)^{-3} x^2 \quad (4.3.11)$$

with the bound $\kappa = 7.746$.

With these two expressions, the respective probabilities of error are written similar to eq.(3.6.2), using which the power penalties are evaluated numerically. Figures (4.5) and (4.6) show the power penalties in these two cases, plotted once again as a function of R , the reflection coefficient, and the corresponding Gaussian and uniform approximations are also shown for comparison. This method is shown to provide the smallest power penalties.

All these approximations make sense only if they are compared to the actual situation. In the following section, a method for estimating the actual probability density function is given.

4.4 The Gram-Charlier Series approximation for the probability density function in the multiple reflector situation

In this section, a technique for estimating the probability function of RIN in a multiple reflector environment is presented. To start off, we repeat eq. (4.3.7) which represents the interferometric noise term when there are N reflectors in the system.

$$x = 2 \cos (\omega_0 \tau_{21} + \Phi(t, \tau_{21})) + 2 \cos (\omega_0 \tau_{31} + \Phi(t, \tau_{31})) + \dots + 2 \cos(\omega_0 \tau_{ij} + \Phi(t, \tau_{ij}) + \dots \quad (4.3.7)$$

The random variable x can also be written as :

$$x = x_1 + x_2 + x_3 + \dots + x_n \quad (4.4.1)$$

where each x_i is also a random variable. Assuming incoherent interference, these random variable are iid : independent and identically distributed. The probability density function of each of these random variables is given by :

$$p_{x_i}(x) = \frac{1}{\pi\sqrt{4 - x_i^2}} \quad (4.4.2)$$

similar to section 3.3. Computing the probability density function of x is not trivial. As n becomes large, the resultant probability density function of x tends to Gaussian, according to the Central Limit Theorem. However, for values of n less than say six or eight the Gaussian approximation is not very accurate. Note that six terms correspond to four reflectors. A method for estimating the p.d.f of x is presented below.

The characteristic function of a random variable is defined to be :

$$G(\omega) = E[\exp(j\omega x)] \quad (4.4.3)$$

where $E[.]$ denotes the expectation operator. The characteristic function of x_i is found to be :

$$G(\omega) = \int_{-\infty}^{\infty} \frac{\exp(j\omega x)}{\pi\sqrt{4 - x^2}} dx = \int_{-\pi}^{\pi} \exp(j\omega 2\cos(\omega_0\tau + \Phi(t,\tau))) d\Phi \quad (4.4.4)$$

which is evaluated to give :

$$G(\omega) = J_0(2\omega)$$

where $J_0(2\omega)$ is the zeroth-order Bessels' function of the first kind. Now, the

characteristic function of the sum of a number of independent random variables is the product of their characteristic functions. Hence, the characteristic function for n reflection terms is given by :

$$G(\omega) = \{ J_0(2\omega) \}^n \quad (4.4.4a)$$

Hence, the probability density function of x can in principle be obtained simply by taking the Fourier transform of its characteristic function and dividing the result by 2π :

$$f_x(x) = \frac{1}{2\pi} \int_{-\infty}^{\infty} G(\omega) \exp(-j\omega x) d\omega = \frac{1}{2\pi} \int_{-\infty}^{\infty} \{ J_0(2\omega) \}^n \exp(-j\omega x) d\omega \quad (4.4.5)$$

We do not believe that this can be done analytically. However, the moments of the distribution can be calculated from the characteristic function. Differentiating (4.4.3) n times,

$$G^{(n)}(\omega) = E \{ j^n x^n \exp(j\omega x) \} \quad (4.4.6)$$

or,

$$G^{(n)}(0) = j^n E(x^n) = j^n m_n \quad (4.4.7)$$

Hence,

$$m_n = (-j)^n G^{(n)}(0) \quad (4.4.8)$$

The moments can then be used in a Gram Charlier series expansion [14] to approximate the probability density function of x :

$$f_x(x) = \frac{1}{\sqrt{2\pi}} \exp\left(-\frac{x^2}{2}\right) \sum C_j H_j(x) \quad (4.4.9)$$

for a distribution having mean = 0 and variance = 1 (which assumption is modified later).

The basis functions of the expansion are the Tchebyeff-Hermite (T-H) polynomials, the first few of which are listed below :

$$\begin{aligned} H_0(x) &= 1 \\ H_1(x) &= x \\ H_2(x) &= x^2 - 1 \end{aligned} \quad (4.4.10)$$

Higher order polynomials may be computed using the recursive relationship :

$$H_k(x) - x H_{k-1}(x) + (k-1)H_{k-2}(x) = 0, \quad k \geq 2 \quad (4.4.11)$$

The C_k s are the coefficients of the series expansion and are expressed in terms of the moments :

$$\begin{aligned} C_0 &= 1 \\ C_1 &= m_1 \\ C_2 &= \frac{1}{2}(m_2-1) \\ &\vdots \end{aligned} \quad (4.4.12)$$

The Gram Charlier series expansion for the pdf of a random variable x with mean μ and variance σ^2 has the form :

$$f_x(x) = \frac{1}{\sigma_x \sqrt{2\pi}} \exp\left(-\frac{(x-\mu_x)^2}{2\sigma_x^2}\right) \sum_{j=0}^{\infty} C_j H_j\left(\frac{x-\mu_x}{\sigma_x}\right) \quad (4.4.13)$$

where the C_j s are given by formulae similar to those in (4.4.12) except that the moments are given by m_n' which are given by :

$$m'_n = E \left\{ \left[\frac{x - m_1}{\sigma_x} \right]^n \right\} \quad (4.4.14)$$

In the case of 3 reflection points, i.e 3 reflection terms, the characteristic function of x is given by :

$$G(\omega) = \{ J_0(2\omega) \}^3 \quad (4.4.15)$$

The moments of x are computed by taking the derivatives of $\{ J_0(2\omega) \}^3$ at $\omega = 0$. Going through the algebra, the moments of the function are as follows :

$$\begin{aligned} m_2 &= 6 ; & m_4 &= 90 \\ m_6 &= 1860 ; & m_8 &= \frac{28920}{7} \end{aligned} \quad (4.4.16)$$

and all the odd moments are zero. Using these, the C_j s are computed. The expression for the probability density function of x is then given by :

$$f_x(x) = \frac{1}{\sqrt{12\pi}} \exp\left(-\frac{x^2}{12}\right) \left\{ \frac{1}{648} \left(\frac{1185}{2} + 21x^2 - \frac{19}{24}x^4 + \frac{x^6}{216} \right) \right\} \quad (4.4.17)$$

With this expression, the probability of error can be fairly easily evaluated numerically, using eq.(3.1.6). Following this procedure, the power penalties incurred in maintaining an error probability of 10^{-9} have been evaluated and are shown in figure (4.5).

The corresponding penalties assuming a Gaussian distribution have also been calculated and are shown in the same figure for comparison. As expected, the Gaussian approximation is more pessimistic.

For four reflection points, number of reflection terms $n = 6$. The characteristic function of x is then given by :

$$G(\omega) = \{J_0(2\omega)\}^6 \quad (4.4.18)$$

Using a similar technique, the moments of the distribution and the coefficients of the Hermite polynomials have been calculated. The probability density function of x is found to be :

$$f_x(x) = \frac{1}{3456} \frac{1}{\sqrt{24\pi}} \exp\left(-\frac{x^2}{24}\right) \left(3328 + 23x^2 - \frac{37}{108}x^4 + \frac{x^6}{1296}\right) \quad (4.4.19)$$

Once again, the power penalties are calculated and the calculations repeated for a Gaussian distribution. These are plotted in Fig.(4.6). Comparing the two figures, it is easily seen that as n increases, the power penalty calculated from the Gaussian distribution is close to that calculated from the actual distribution.

A comment on the Gram-Charlier Series expansion method : an obvious question that arises while using this technique is the number of terms that need to be included. According to [14], this series is most useful while approximating the density functions of random variables that are the sums of independent random variables . Further, the series unfortunately does not converge uniformly. Hence including a larger number of terms does not automatically imply better results. A rule of thumb in practical applications is to consider around six terms. In this case, the odd moments are all zero. However, the fact they are zero are characteristic of the probability density function, even though at first sight it might appear that we have considered only four terms.

Comparing the Gram-Charlier series approximation with the uniform and quadratic approximations, we see that as the number of reflectors increases, the results with these approximations become increasingly optimistic. That is, with an increasing number of reflectors, the resultant p.d.f becomes more Gaussian, as a result of which the uniform and quadratic approximations are no longer as useful in predicting the power penalties. This is illustrated in the case of three and four reflectors. For three reflectors, the uniform and quadratic approximations provide better results than the Gaussian approximation, relative to the exact calculation. However, for four reflectors, the resultant p.d.f becomes more Gaussian, and we see (fig.4.6) that the uniform and quadratic approximations in fact predict a lesser power penalty than the exact calculation.

5.0 Low frequency enhancements in the spectrum of RIN

As mentioned in section 3.1, the experimental results of Gimlett and Cheung [6] show that there is a greater low frequency content in RIN than the calculations in that section predicted. These discrepancies can be noticed by examining figure (2.2). In this chapter, an outline of a model that at least partially explains these discrepancies is presented. The results in chapter 3, as well as prior literature, were calculated assuming a Lorentzian line shape for the laser linewidth. A Lorentzian line shape corresponds to an instantaneous frequency noise that has a white spectrum. We show here that a low frequency dip in the spectrum of the instantaneous frequency noise (possibly caused by thermally induced phase modulation) leads to an increase in the low frequency spectrum of reflection induced noise consistent with measurement.

5.1 Low frequency variations

As mentioned earlier (section 3.1), the phase variations $\phi(t)$ of a single longitudinal mode laser are typically modeled as a random walk process in which the phase change $\Delta\phi$ over the time t has a density function which is a Gaussian with zero mean and variance given by $\sigma^2(\tau) = \tau / \tau_c$, where τ_c is the coherence time of the laser. In the frequency domain, this leads to the familiar Lorentzian shaped line with a full width half maximum (FWHM) linewidth $\Delta\nu$ given by :

$\Delta\nu = 1 / 2\pi\tau_c$. This is also equivalent to taking $d\phi / dt$ (which can be termed the instantaneous frequency noise) to be a white noise Gaussian process with a two-sided spectral density given by $2\pi\Delta\nu$. This is proved in the following paragraph.

The change in phase $\Delta\phi$ in time period τ starting from any arbitrary time instant t_0 is given by :

$$\Delta\phi = \int_{t_0}^{t_0 + \tau} dt \dot{\phi} \quad (5.1.1)$$

where $\Delta\phi(\tau)$ is also a zero mean Gaussian process.

The variance $\langle (\Delta\phi)^2 \rangle$ is given by :

$$\langle (\Delta\phi)^2 \rangle = \int_{t_0}^{t_0 + \tau} \int_{t_0}^{t_0 + \tau} dt dt' \langle \dot{\phi}(t) \dot{\phi}(t') \rangle \quad (5.1.2)$$

But, for white noise, the autocorrelation $\langle \dot{\phi}(t) \dot{\phi}(t') \rangle$ is, by definition, given by [12] :

$$\langle \dot{\phi}(t) \dot{\phi}(t') \rangle = 2\pi (\Delta\nu) \delta(t - t').$$

Hence, the variance is given by :

$$\begin{aligned} \langle (\Delta\phi)^2 \rangle &= 2\pi\Delta\nu \int_{t_0}^{t_0 + \tau} dt \\ &= 2\pi\Delta\nu\tau, \quad \tau \geq 0 \end{aligned} \quad (5.1.3)$$

Replacing τ by $|\tau|$ on the right hand side of eq.(5.1.3) generalizes the result to apply for all τ .

In this simple model of phase variation, turn-on and turn-off transients have been neglected, which become increasingly important at high bit rates. Such effects are best handled by using the basic laser rate equations. These features are outside the scope of this thesis but this is an area of possible future work.

In section 3.1, it was shown that for the case of a single interferometer, i.e. two reflectors, with a round trip delay between the reflectors long compared to the laser coherence time (i.e. the incoherent case), the power spectrum of the reflection noise is simply related to the power spectrum of the laser. There is good agreement between the theoretically predicted results and the experimentally obtained results except at very low frequencies (below about 10 MHz) where the measurements seem to indicate that a narrowband low frequency line is superimposed on the wideband Lorentzian line. A

plausible explanation for this phenomenon is given below.

In the incoherent case, the power spectrum of the reflection induced noise reduces to the form (the details are given in Appendix A) , after scale factors have been neglected :

$$P(\omega) = \int_{-\infty}^{\infty} d\tau \exp(-\sigma^2(\tau) - j\omega\tau) \quad (5.1.4)$$

Note that τ here is the running variable of integration and not a fixed time delay. The spectrum is independent of the delay time when the delay time is large compared to the coherence time of the source. $P(\omega)$ is the Fourier transform of $\exp[-\sigma^2]$, while the optical spectrum is given by the Fourier transform of $\exp[-\sigma^2/2]$. In other words, in the incoherent case, the spectrum of RIN is obtained by convolving the laser line spectrum with itself. Self-convolution of a Lorentzian spectrum results in a Lorentzian line spectrum. This shape preserving feature is not generally true for other line shapes.

To explain the enhanced content of the low frequency component in RIN, we deviate from the Lorentzian line shape assumed for the laser. That is, we assume that the phase change and variance are not described by equations (5.1.1) - (5.1.3). Instead, we assume that the power spectrum of the instantaneous frequency of the laser is given by :

$$H(\omega) = 2\pi(\Delta\nu) \left[1 - \frac{\kappa\omega_0^2}{\omega^2 + \omega_0^2} \right] \quad (5.1.5)$$

The second term in this equation corresponds to a low frequency dip in the spectrum of the instantaneous frequency. This is assumed to be plausible because the spectrum of the instantaneous frequency is shaped by the FM response of the laser, which in turn is known to have a low frequency dip associated with thermal phenomena [15]. The parameter κ (≤ 1) determines the magnitude of the dip, and ω_0 is the corner frequency.

The Fourier transform of eq.(5.1.5) gives the autocorrelation function of the instantaneous frequency. The case $\kappa = 0$ corresponds to the Lorentzian line shape, whose autocorrelation function is the delta function mentioned earlier in this chapter. The autocorrelation function $h(t - t')$ for general κ is given by the Fourier transform of eq.(5.1.5):

$$h(t - t') = 2\pi\Delta\nu \delta(t) - \pi\Delta\nu\kappa\omega_0 \exp(-\omega_0|t - t'|) \quad (5.1.6)$$

From this, the variance $\sigma^2(\tau)$ is found to be :

$$\langle(\Delta\phi)^2\rangle = 2\pi\Delta\nu\tau - (2\pi\Delta\nu\kappa\omega_0) \int_0^\tau dt \int_0^\tau dt' \exp[-\omega_0|t - t'|] \quad (5.1.7)$$

or,

$$\langle(\Delta\phi)^2\rangle = 2\pi\Delta\nu [1 - \kappa] \tau + \frac{2\pi\Delta\nu\kappa}{\omega_0} (1 - \exp(-\omega_0\tau)) \quad (5.1.8)$$

This expression has the following limiting forms :

$$\begin{aligned} \sigma^2(\tau) &\approx 2\pi\Delta\nu\tau & \text{for } \omega_0\tau \ll 1 \\ \sigma^2(\tau) &\approx 2\pi\Delta\nu(1 - \kappa)\tau + \frac{2\pi\Delta\nu\kappa}{\omega_0} & \text{for } \omega_0\tau \gg 1 \end{aligned} \quad (5.1.9)$$

In both these limits, the variance is linear in τ . This leads to Lorentzian line spectra

with a high frequency (small τ) behavior determined by the linewidth $\Delta\nu$, and a low frequency behavior determined by a reduced linewidth $(1 - \kappa)\Delta\nu$. However, for the deviations from the Lorentzian spectrum to be significant, κ should approach unity and $\omega_0\tau_c$ should not be too small. This is shown in fig.(5.1) where the power spectrum at zero frequency is plotted as a function of $\omega_0\tau_c$ (denoted by γ) for several values of κ (the DC spectrum is normalized to unity for $\kappa = 0$). The former condition implies that thermal phase modulation be comparable to the carrier induced effects (they are 180 degrees out of phase [15]), and the latter requires that the corner frequency, $\omega_0/2\pi$, be comparable to, or greater than, the laser linewidth. This implies that significant low frequency deviations from the Lorentzian spectrum may be expected only in lasers with linewidths of the order of 10 MHz or less.

To illustrate the low frequency effects when the above conditions apply, σ^2 is plotted in figure (5.2) as a function of τ / τ_c , for various values of κ , but for fixed $\gamma \equiv \omega_0\tau_c = 1$.

The power spectral density of RIN is calculated as follows :

$$\begin{aligned}
 P(\omega) &= \int_{-\infty}^{\infty} d\tau \exp(-\sigma^2(\tau)) \exp(-j\omega\tau) \\
 &= \tau_c \int_{-\infty}^{\infty} du \exp(-\sigma^2(u)) \exp(-j\omega\tau_c u)
 \end{aligned} \tag{5.1.10}$$

where u is the normalized variable $= \tau / \tau_c$. Letting $x = \omega\tau_c$, the expression for the power spectral density can be written in a form suitable for numerical evaluation, in the derivation

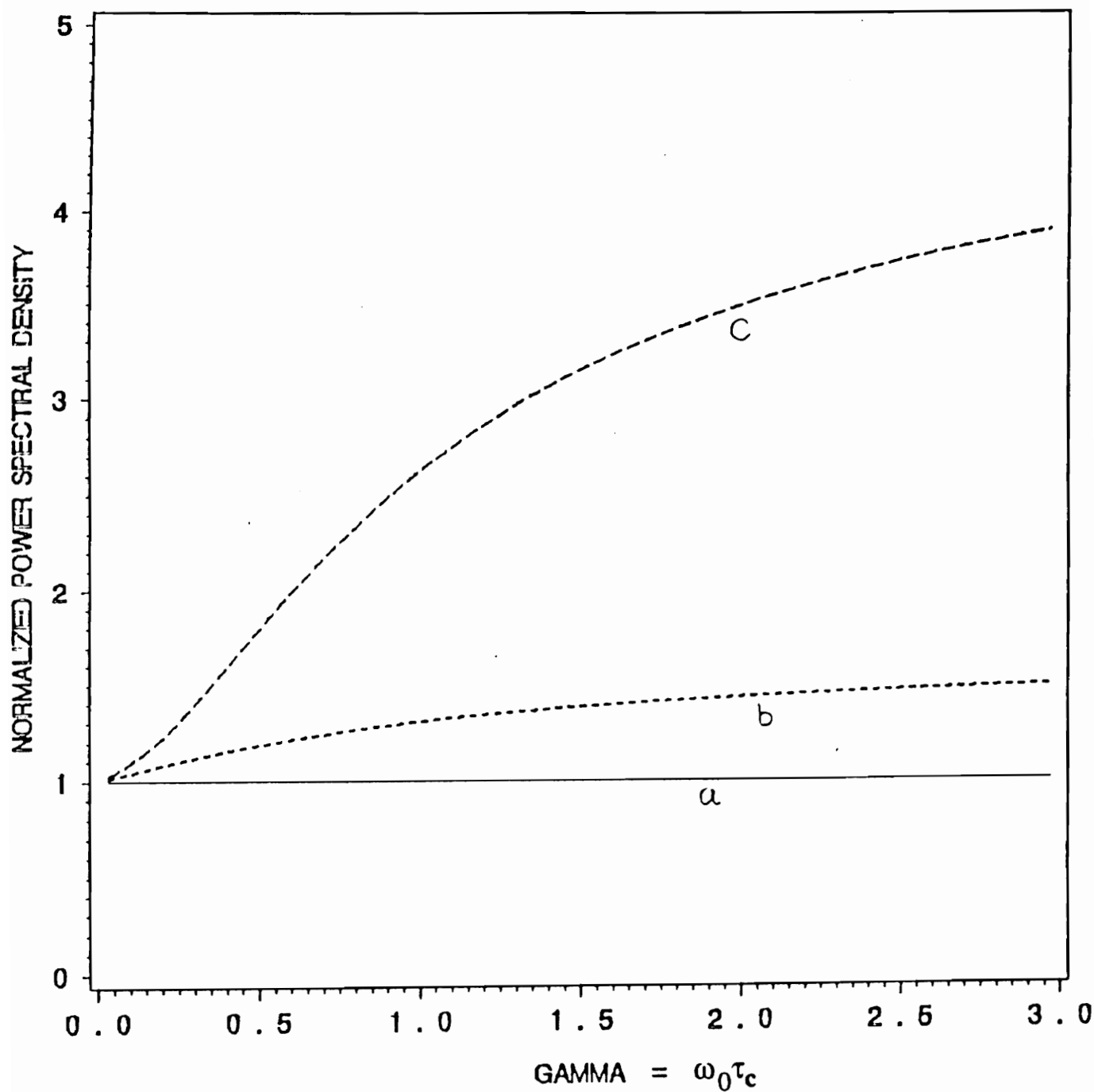


Fig. 5.1 DC values of normalized power spectrum of RIN as a function of $\gamma = \omega_0 \tau_c$:
a) $\kappa = 0$ b) $\kappa = 0.4$ c) $\kappa = 0.8$

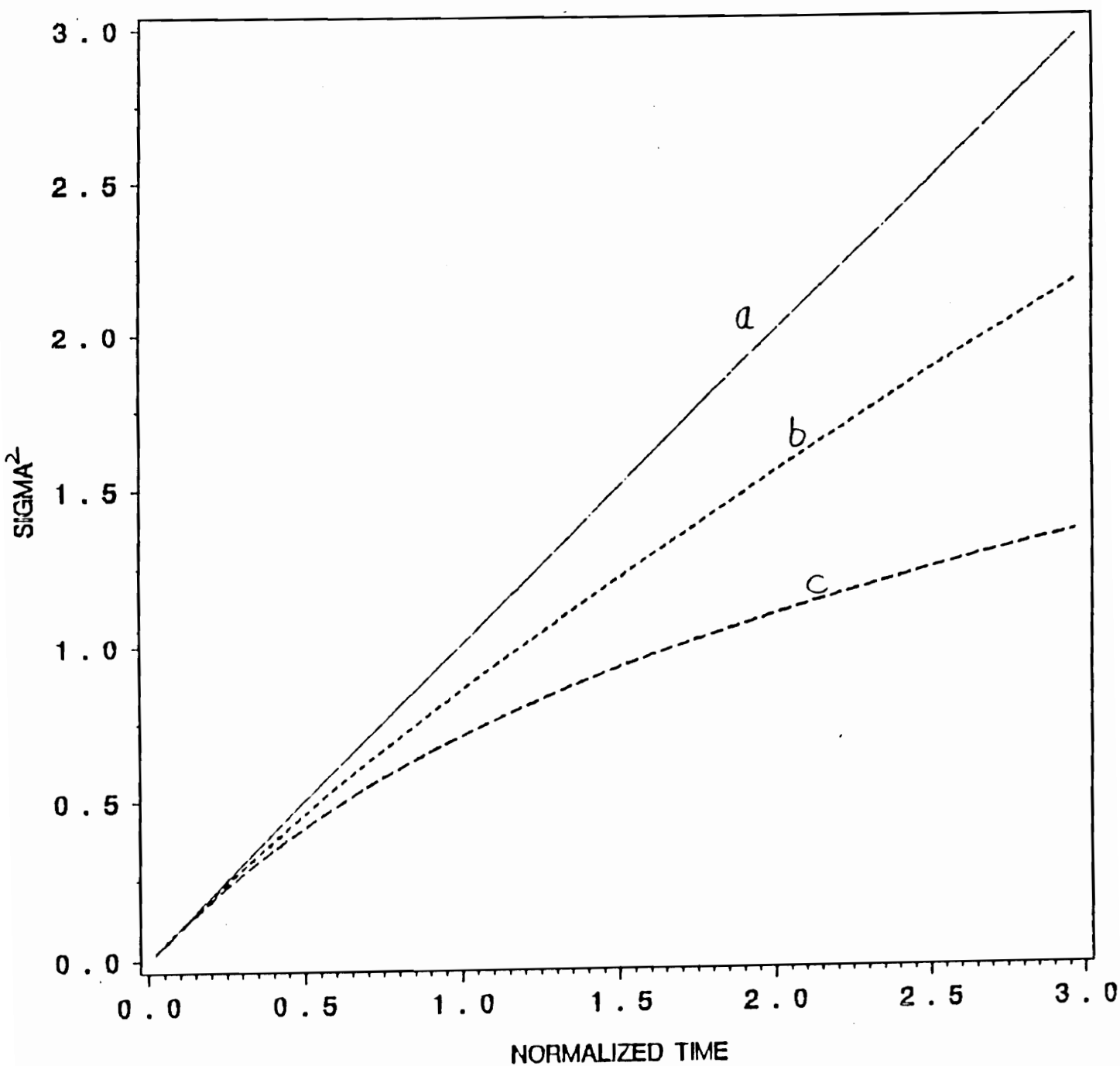


Fig. 5.2 σ^2 as a function of normalized time τ/τ_c for $\gamma = 1$:
a) $\kappa = 0$ b) $\kappa = 0.4$ c) $\kappa = 0.8$

of which the evenness of the function $\sigma^2(u)$ has been utilized :

$$P(x) = \int_0^{\infty} du \exp(- (1-\kappa)u) \exp(- \frac{\kappa}{\gamma} (1 - \exp(- \gamma u))) \cos xu \quad (5.1.11)$$

Results obtained from the numerical evaluation of eq.(5.1.11) are plotted in fig.(5.3) as a function of x for various values of κ and for $\gamma = 1$. It is easily seen that the above equation reduces to the Lorentzian line shape for $\kappa = 0$. For $\kappa > 0$, fig. (5.3) indeed indicates an increase in the noise at low frequency relative to that calculated from a single Lorentzian line, for example, when $\kappa = 0.8$, there is a 4.2 dB peaking in the low frequency spectrum.

5.2 Discussions

Although it has been analytically shown that there is a connection between the low frequency rise in the spectrum of the reflection induced noise and a low frequency dip in the spectrum of the instantaneous frequency noise, a detailed analytical justification of the latter has not been provided. Hence, it would be very desirable to verify both analytically and experimentally the presumed relation between the instantaneous frequency noise and the FM response of the laser. Comparison of measurements with the same laser of reflection induced noise and the FM response would provide a test of the above supposition. If successful, this would then enable measurements of reflection induced noise to be used as a means of characterizing the FM response of single longitudinal mode lasers.

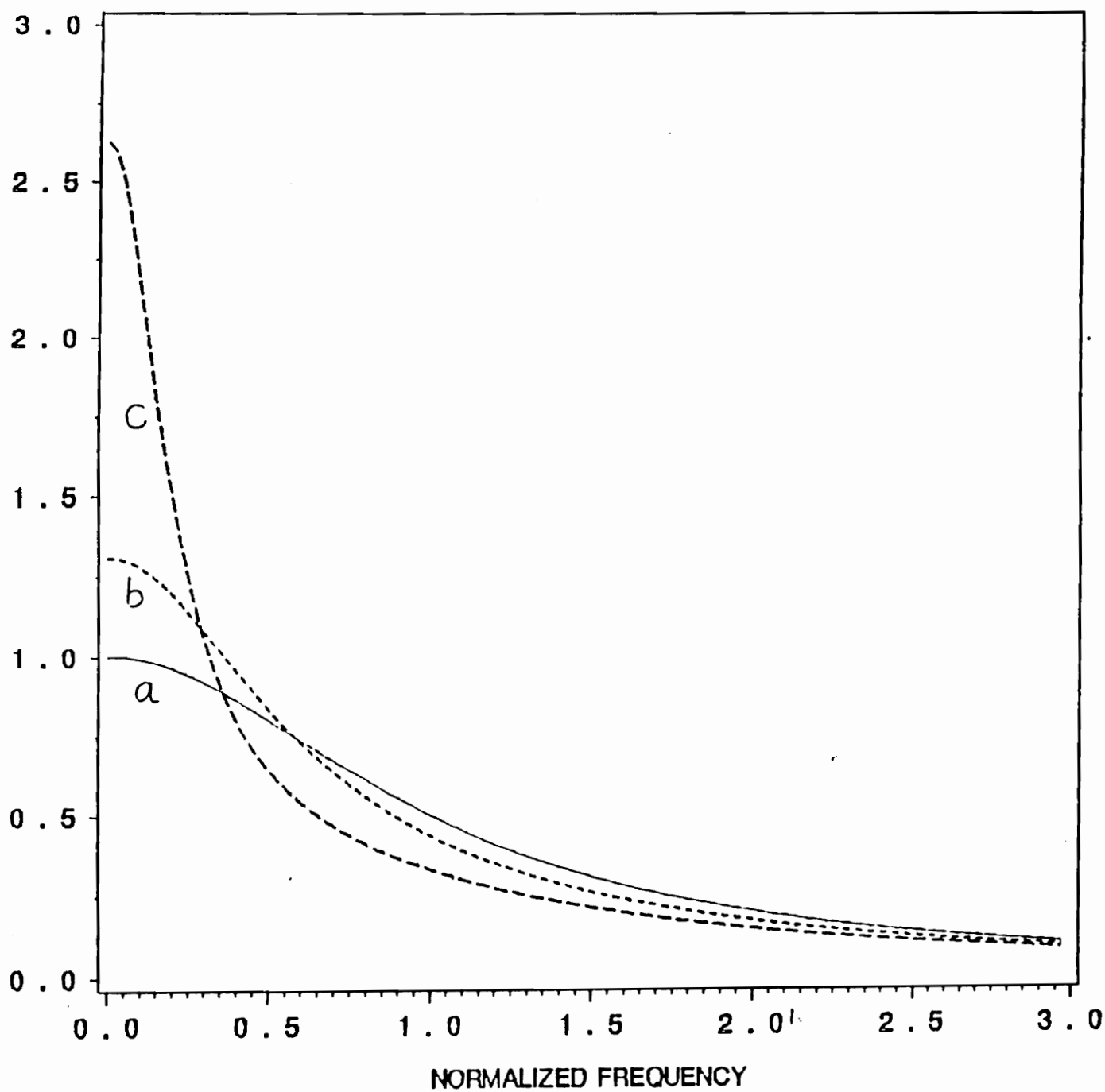


Fig. 5.3 Low frequency enhancement in the power spectrum of RIN plotted vs. normalized frequency $\omega\tau_c$ for $\gamma = 1$
a) $\kappa = 0$ b) $\kappa = 0.4$ c) $\kappa = 0.8$

6.0 Physical modeling

So far, the analysis of reflection induced noise has been done by considering a fixed reflectivity at the refractive index discontinuities along the fiber transmission line. The physical causes and nature of these discontinuities have not been considered in the analysis. The discrete reflectivities described by fixed numbers do not offer much insight into the physical nature of these reflectors, knowledge of which is essential to take measures to minimize their impact on system performance. Further, all the randomness in this phenomenon is described by the random variable x , in the formalism developed in chapter 3. There are various factors that affect the probability density function of x . The coding scheme employed in the transmission system is one example. In this chapter, we touch on the relationship between the parameters in our model and physical parameters in actual systems.

6.1 Reflections from splices and connectors

Optical energy is reflected towards its source at splices and connectors. The effects of a given reflection coefficient have been considered in some detail in the preceding chapters. In this section, we discuss the relation of reflection coefficients to some of the physical parameters characterizing splices and connectors.

Splices are considered first. The amount of optical energy reflected from a non-fusion splice depends on three factors [16]:

- a) the quality of the fiber endface
- b) the closeness of the index matching to the fiber's index of refraction
- c) the spacing between the two fiber ends.

In particular, the degree of polish on the end of a fiber has a substantial effect on reflection even when the end is immersed in an oil whose index of refraction matches that of the fiber extremely well. Further, even in single mode systems, splices generate modal noise that affects the BER. This phenomenon has been extensively studied and can cause difficulties under certain circumstances. However, it can be eliminated fairly easily in practical systems [17]. The effects of these reflections is very small if the reflection coefficients are less than 1%. It is expected that coherent systems will require even lower levels of reflection.

In the case of connectors, the situation is similar. To reduce the reflection effects, fiber joints are designed to have physical contact, are index matched, or have tilted endfaces [18]. In fiber joints designed for endface contact, an air gap between fiber endfaces may still exist due to either the non-perpendicularity of endfaces or the presence of contaminants or design tolerances. Also, in convex polished connectors, physical contact may occur away from the core owing to off-axis polishing. Recent work by Shah et. al [1] has shown that the polishing of fiber endfaces may substantially increase the refractive index of the surface from 1.47 to about 1.6. This region of higher index, about 0.15 microns deep, results in interference effects that can cause reflection losses of greater than 1.1 dB, which

is greater than the maximum specified loss for some connectors. Fig. (6.1) [18] shows the effect of small changes in the air gap length between two single mode fibers on the coupling efficiency of a connector having polished end faces. In the following section, an outline of the theory describing the influence of a random air gap on fiber transmittance is presented.

6.2 Reflections from non contacting joints

Wagner and Sandahl [19] have performed a detailed analysis of the transmission characteristics of fiber connections. Non contacting fiber connectors have a small air gap, which can be modeled by a Fabry-Perot cavity. Multiple reflections within the cavity produce interference effects which are observed as transmission fluctuations if either the fiber separation or the source wavelength is varied. These effects occur provided the fiber separation is less than the coherence length of the source. Since the air gaps cannot be predicted to be of a fixed length, statistical techniques must be employed in their analysis.

The reflection coefficient for a Fabry Perot cavity is given by [20]:

$$R_{\text{eff}} = \frac{4R \sin^2 \delta}{(1 - R)^2 + 4R \sin^2 \delta} \quad (6.2.1)$$

where

$$\delta = \pi \Delta d / \lambda_c \quad \text{and} \quad R = (n - 1 / n + 1)^2 .$$

n is the refractive index of the fiber, λ_c the center wavelength of the laser, Δd is the width of the air gap, and R is the reflectivity of the boundary between the air and fiber endface. As mentioned, Δd is not fixed. Assuming that it is uniformly distributed, the probability

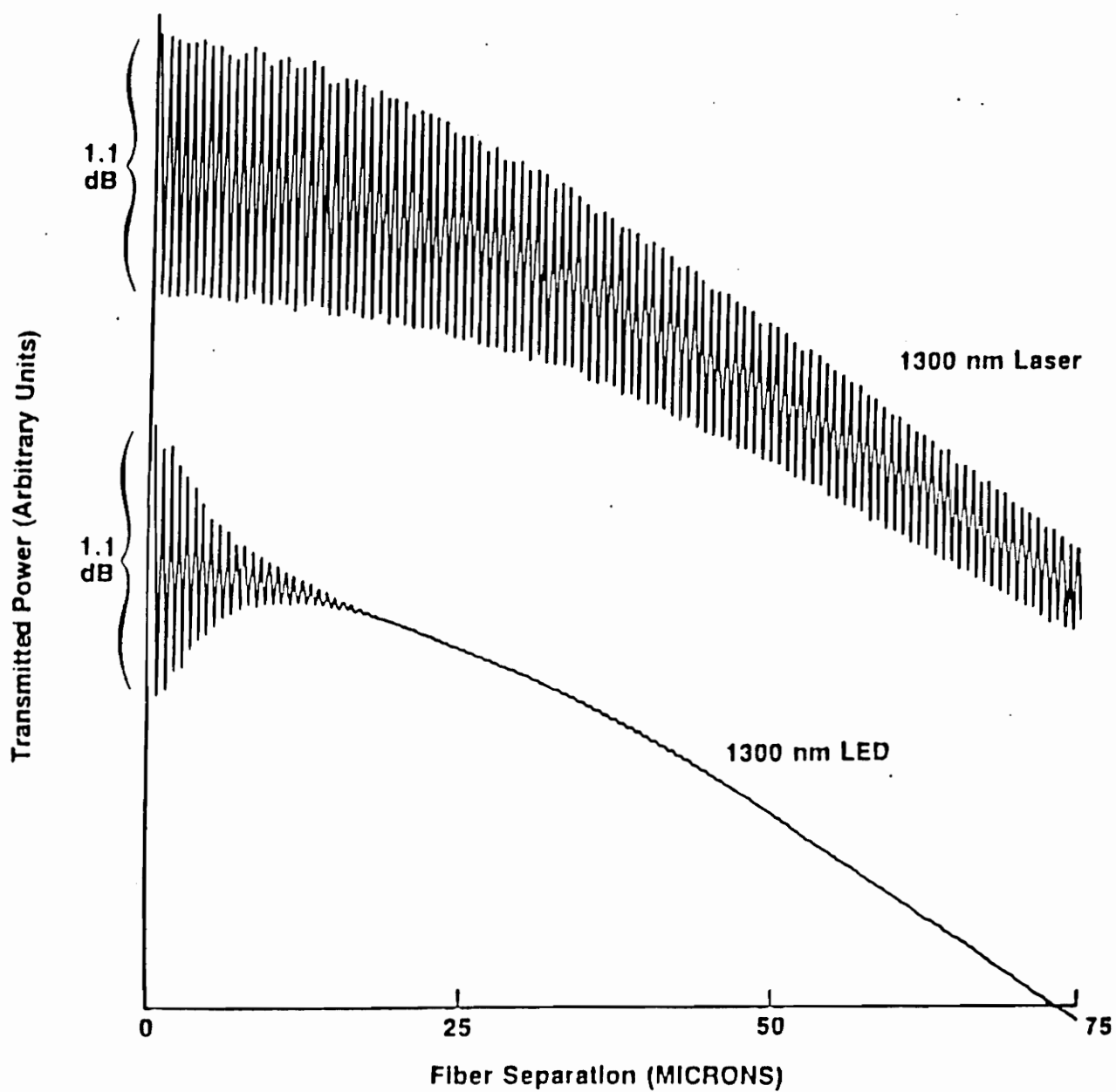


Fig. 6.1 Transmission vs. fiber end separation for a single mode fiber at a wavelength of 1300 nm. (taken from ref.[18])

density function for a given reflectivity R_{eff} is given by :

$$P(R_{eff}) = \frac{\sqrt{1 - R_{max}}}{\pi(1 - R_{eff})\sqrt{R_{eff}(R_{max} - R_{eff})}} \quad (6.2.2)$$

where $R_{max} = 4R / (1 + R)^2$. Using this equation, Fishman et al [20] have found that for $n = 1.45$ to 1.57 , the maximum reflection R_{max} varies from 12.6% to 17.9% and the mean reflection from 6.53% to 9.3% . The relation for the probability density function is used to derive a probability density function for the R used so far in this document, which has been defined to be the geometric mean of the reflectivities of the two discontinuities. In fact, it is the geometric mean of the reflectivities of two random air gaps. The resultant probability density function is a convolution integral that has been evaluated numerically. The resulting distribution has a mean varying from 5.5% to 8.3% and a maximum varying from 12.6% to 17.9% , as the refractive index varies from 1.45 to 1.57 . Thus for $n = 1.57$, the mean reflection coefficient resulting from two lossless non-contacting connections is 8.3% . The power penalty from RIN corresponding to this value of the mean reflection coefficient is 1.4 dB (from fig. 3.2). Hence, a system with only two non-contacting connectors will have a mean power loss of 1.4 dB, neglecting jumper loss etc. This shows that the power penalties incurred are fairly heavy, and may be unacceptable in power limited fiber optic systems.

All this shows that attention needs to be paid to the design of connectors and splices such that these reflections are minimized. It should be noted that these reflections can be minimized by using an index matching medium (fluid / gel) etc. between the fiber end faces and while this approach is common in the splicing of fibers, due to considerations like cleanliness and contamination, it is usually not used in demountable connectors. In such cases, however, the connectors can be polished at an angle such that the reflected power is not guided into the fiber. Drake [21] has studied various types of fiber end terminations and connections. He has listed some of the better terminations and connections - those which have low reflectance properties. The double-bulb connector, drawn in fig.(6.2), according

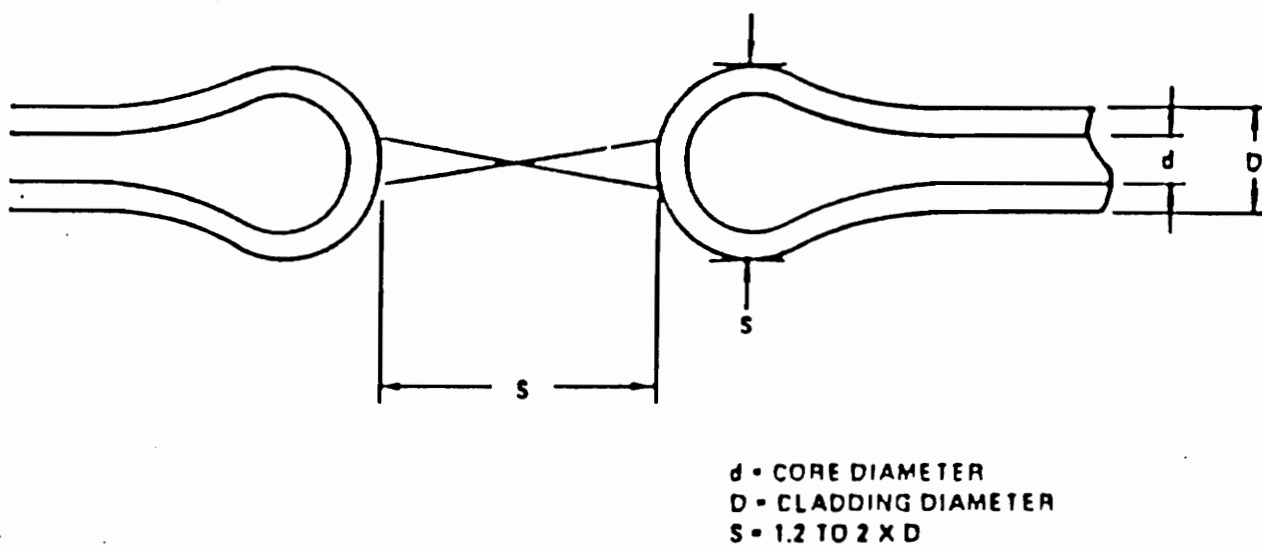


Fig. 6.2 **Concept of a double bulb connector**
 (taken from ref.[21])

to him, is one type that has a low reflectance (less than 1%).

6.3 Coding effects on RIN

As mentioned previously (section 3.1), the statistics of RIN are influenced by the line coding schemes employed. The analysis thus far had been done with NRZ formatted data. Elrefaie et al [22] have considered return-to-zero formatted data and have evaluated the performance degradations due to RIN using computer simulation techniques. Basically, the single mode laser rate equations were solved numerically to obtain the statistics of the phase fluctuations. The simulations were done for both NRZ and RZ line coding schemes. It was found that the RZ performance was better by about 1.0 dB than NRZ at a error rate of 10^{-9} . The power penalties are shown in fig.(6.3) as a function of the round trip delay between the joints. The power penalty of the NRZ system varies slowly with the delay time t , while the RZ penalty peaks only at values of t equal to an integer number of bits. For instance, in the case where both connectors have 8 dB return loss (i.e. a reflection coefficient of about 15%), at round trip delays equal to an integer number of bits, the power penalty of both NRZ and RZ systems is 3 dB. However, at offset delays, although the power penalty of the NRZ system remains at 3 dB, the RZ penalty is reduced to 1.5 dB. The value of the return loss represents a worst case situation. For lightwave systems with multiple connectors, the RZ system penalty is found to be sensitive to the distance between connectors and in the worst case is equal to the NRZ system penalty.

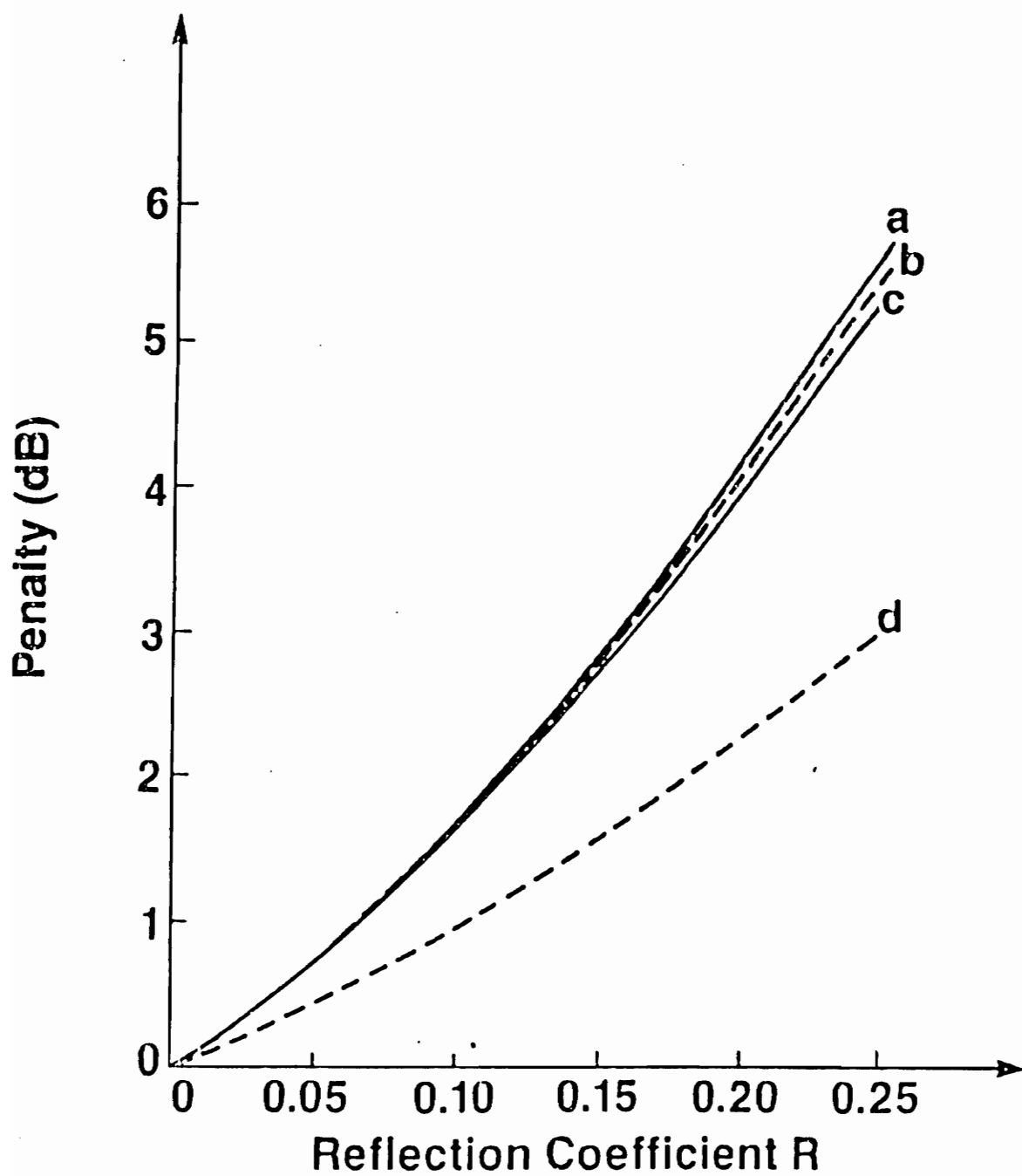


Fig. 6.3 Power penalty vs. reflection coefficient R for :
a) NRZ, $\tau = 40$ bits, b) RZ, $\tau = 40$ bits
c) NRZ, $\tau = 40.5$ bits, d) RZ, $\tau = 40.5$ bits
(taken from ref.[22])

7.0 Conclusions

7.1 Summary

Reflection induced noise in fiber optic systems due to the presence of refractive index discontinuities is an example of signal dependent noise in a communications system. It is an impairment that has always been present in fiber systems. However, it is only recently that there has been any significant interest in it - with the advent of high speed systems and narrow linewidth lasers. It is recognized as an important factor in determining overall system performance.

The work in this thesis can be broadly divided into two categories :

- a) study of RIN as a specific impairment in a fiber communication system
- b) development of a methodology for evaluating the effects of signal dependent noise.

This thesis, in addition to summarizing the broad literature on this subject, has made new contributions on the following topics :

- i) multiple reflections at a single pair of reflectors
- ii) multiple reflectors in the system
- iii) presence of other impairments in the system
- iv) enhanced low frequency content in the spectrum of RIN.

The effects of signal dependent noise in a communications system do not generally lend themselves to easy analytical solutions. Primarily, the probability density functions of the random variables representing such phenomena are not easy to evaluate. They, in general, do not fit into the Gaussian model which is much more amenable to analysis. A major part of this thesis has concerned itself with ways to estimate the probability density function and the corresponding power penalty in such situations. We have come up with a few simple models which have provided accurate estimates of the power penalty incurred in maintaining a nominal error probability. It must be reiterated here that while these approximations are not very useful in predicting actual error probabilities, the quantity that is often of greater interest, especially in power limited fiber systems, is the power penalty that must be paid to maintain a nominal error probability.

7.2 Conclusions and principal contributions

In chapter three, we show that a degradation like RIN that is bounded does not result in a BER floor. The uniform and quadratic approximations for the probability density function of RIN provide good estimates of the power penalty relative to an exact calculation. The analysis shows that as long as the approximation considered has the same bounds as the actual p.d.f, the power penalties are in excellent agreement, even though the shapes of the two distributions may be very different. In fact, owing to the steepness of the p.d.f of RIN, it has been approximated as an eye degradation equal to the maximum value of the noise, with good results.

In the case of a multiplicity of reflectors in the system, the p.d.f of the resultant noise process cannot be evaluated analytically. However, since the moments may be calculated, the Gram-Charlier series method is used to estimate the p.d.f of the process. The power penalty incurred in maintaining a 10^{-9} error probability is then calculated. We have shown that the power penalties increase rapidly with the reflectivity R . We see that the reflectivities must be less than a few percent (2-3%) to ensure acceptable levels of degradation. Further, as the number of reflectors increases, the p.d.f of the resultant noise process tends to become more Gaussian, keeping with the predictions of the Central Limit Theorem. For three reflectors, there is a significant difference between the Gaussian approximation and the actual p.d.f (the Gram-Charlier series approximation). However, for four reflectors, there is not much difference between the two. As the number of reflectors increases, the uniform and the quadratic approximations also become increasingly inaccurate as the pdf tends to become Gaussian.

The discrepancies between theoretically calculated and experimentally measured power penalties were sought to be resolved by considering effects that had been neglected in the literature. The effects of multiple reflections and the presence of an extinction ratio (or other fixed degradations) are two possibilities that at least qualitatively explain the discrepancies. We have shown that indeed these effects do result in higher power penalties, in keeping with the experimental results.

The enhanced low frequency content in the spectrum of RIN observed in the literature is explained by postulating a low frequency dip in the spectrum of the instantaneous frequency noise, which is probably caused by thermal phase modulation. We show that this indeed indicates an increase in the noise at low frequency relative to that calculated from a laser with a purely Lorentzian line.

Finally, it may be noted that the power spectrum of RIN in a controlled incoherent situation (a Mach-Zehnder interferometer for example) provides a simple method to measure the linewidth of the laser without having to use complicated optical spectrum analyzers.

7.3 Suggestions for future research

In this thesis, laser phase noise has been characterized by some parameters that are assumed constant, independent of the modulation. In practice, turn-on and turn-off transient effects are extremely important in gigabit per second systems. In this context, we feel that the phenomenon of frequency chirp will have a major impact on RIN and is, in our opinion, worth looking into.

Another area that needs investigation is the impact of RIN on FSK systems. With coherent systems becoming increasingly important, and with their intrinsic sensitivity to random phase variations, an effect like RIN warrants investigation. Once again, these are primarily related to the physical modeling. The methodology presented in this thesis should be applicable.

The impact of coding schemes needs to be looked at in greater detail.

To model these and other effects, the laser rate equations should provide a logical starting point and complex simulations may have to be performed to understand their impact on RIN.

With regard to the wider problem of signal dependent noise, it is of interest to see how broadly the simple approximations developed in this thesis are useful. Specifically, it would be desirable to establish conditions under which the various approximations to the distribution of signal dependent noise are applicable.

Appendix A : Power spectral density in the incoherent case

The autocorrelation function of RIN in the general case is given by eq.(2.3.5) which is reproduced here :

$$R(t, \tau) = 2 R^2 \begin{cases} \exp(-2\pi\Delta\nu|t|) [1 + \cos 2\omega_0\tau \cdot \exp(-4\pi\Delta\nu(\tau - |t|))], & |t| < \tau \\ \exp(-2\pi\Delta\nu\tau) [1 + \cos 2\omega_0\tau] & |t| > \tau \end{cases} \quad (2.3.5)$$

In the incoherent case, $\tau \gg \tau_c$ i.e. the delay time is much greater than the coherence time of the laser. In this regime, the contribution to the autocorrelation function is mostly from the first term in eq. (2.3.5). This is proved as follows :

In this regime, $2\pi\Delta\nu\tau \gg 1$. Hence, $\exp(-2\pi\Delta\nu\tau)$ is negligible, which means that the contribution to the autocorrelation from the second line (when $|t| > \tau$) is negligible. Coming back to the first line, $\tau \gg \tau_c$, $\tau - |t| \gg \tau_c$ most of the time. And since there is an additional factor of 2 in the exponent, the contribution from that term too is not very significant. Hence, the autocorrelation function in the incoherent regime is given by the simpler expression :

$$R(t, \tau) = \exp(-2\pi\Delta\nu|t|) \quad (A.1)$$

neglecting scale factors.

The power spectral density of RIN is then written in the form :

$$P(\omega) = \int_{-\infty}^{\infty} dt \exp(-2\pi\Delta\nu|t| - j\omega t) \quad (\text{A.2})$$

which is similar to eq.(5.1.4) of chapter five, except for the change in the variable of integration. Hence, in the incoherent regime, the power spectral density of RIN is nothing but the Lorentzian line convolved with itself.

Appendix B : Approximation of an exponential probability density function by a quadratic

In keeping with the emphasis placed on the approximation of the probability density functions of signal dependent noise in this thesis, we test our approximation against another known probability density function. We see how good a quadratic approximation is to an exponential probability density function.

A two-sided exponential probability density function is given by [10] :

$$p_x(x) = \frac{\beta}{2} \exp(-\beta|x|) \quad (\text{B.1})$$

whose variance is given by :

$$\sigma^2 = \frac{2}{\beta^2} \quad (\text{B.2})$$

In accordance with the formalism developed in chapter 3, the signal at the receiver decision point is given by :

$$y = a + xRa + n \quad (\text{B.3})$$

where x is the random variable having an exponential distribution. The probability of error is given by eq. (3.1.6) which boils down to the following expression in this case :

$$P_E = \frac{1}{\sqrt{2\pi}} \int_{-\infty}^{\infty} du \exp(-\frac{u^2}{2}) \int_{\frac{1}{2R}(1 - \frac{u}{\alpha})}^{\infty} dx \frac{\beta}{2} \exp(-\beta|x|) \quad (\text{B.4})$$

This expression is evaluated to give :

$$P_E = \frac{1}{2} \exp\left(\frac{\beta}{2R} \left(\frac{1}{4R\alpha^2} - 1\right)\right) \left\{ 1 - Q\left(\alpha - \frac{\beta}{2R\alpha}\right) \right\} - \frac{1}{2} \exp\left(\frac{\beta}{2R} \left(\frac{1}{4R\alpha^2} + 1\right)\right) Q\left(\alpha + \frac{\beta}{2R\alpha}\right) + Q(\alpha) \quad (B.5)$$

In both these expressions, the symbols are as defined in chapter 3. The power penalties can then be evaluated numerically from eq.(B.5).

We try to approximate the power penalty by a quadratic having the same variance as this exponential function. The p.d.f of the quadratic is given by :

$$f_x(x) = a_0 + a_2 x^2, \quad \text{for } -\kappa \leq 0 \leq \kappa \quad (B.6)$$

The unknown a_0 , a_2 and κ are calculated by matching the variance and ensuring that the other conditions mentioned in chapters 3 and 4 are satisfied :

$$a_0 = 0.75 \left(\frac{\beta}{\sqrt{10}}\right); a_2 = -0.75 \left(\frac{\beta}{\sqrt{10}}\right)^3; \kappa = \frac{\sqrt{10}}{\beta} \quad (B.7)$$

Choosing different values of β between 25 and 50 and for high values of R , we numerically evaluate the power penalty incurred in maintaining an error probability of 10^{-9} with this approximation.

Comparing the results with the actual values obtained from eq.(B.5), we find that there is a poor match. We believe that the reason for the poor match is because the exponential has a very long tail, as a result of which there is an error floor. However, since the quadratic approximation is bounded, there is no error floor. Nevertheless, this tells us that the approximations we are considering are not valid in every case. Hence, there is some interest in finding out the conditions under which these approximations hold and also in finding other approximations that give satisfactory results in other circumstances.

References

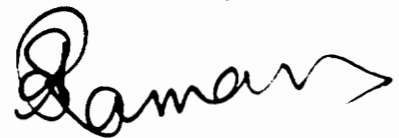
1. V.S. Shah, W.C. Young, and L. Curtis, "Large fluctuations in transmitted power at fiber joints with polished endfaces," *Technical Digest of OFC / IOOC*, Reno, Nevada, 1987, pap. TUF4.
2. J.A. Armstrong, "Theory of interferometric analysis of laser phase noise," *J. Opt. Soc. Amer.*, vol. 56, pp. 1024 - 1031, 1966.
3. K. Petermann and E. Weidel, "Semiconductor laser noise in an interferometric system," *IEEE J. Quant. Electron.*, vol. QE-17, pp. 1251 - 1256, 1981.
4. M.M. Choy, J.L. Gimlett, R. Welter, L. G. Kazovsky, and N. K. Cheung, "Interferometric conversion of laser phase noise to intensity noise by single-mode fiber optic components," *Electron. Lett.*, vol. 23, pp. 1151 - 1152, 1987.
5. J.L. Gimlett, J. Young, R.E. Spicer, and N.K. Cheung, "Degradations in gigabit / sec DFB laser transmission systems due to phase-to-intensity conversion by multiple reflection points," *Electron. Lett.*, vol. 24, pp. 406 - 408, 1988.
6. J.L. Gimlett and N.K. Cheung, "Effects of phase-to-intensity noise conversion by multiple reflections on gigabit-per-second DFB laser transmission systems," *J. Lightwave Technol.*, vol. LT - 7, no. 6, pp. 888 - 895, June 1989.
7. R.W. Tkach and A.R. Chraplyvy, "Phase noise and linewidth in an InGaAsP DFB laser," *J. Lightwave Technol.*, vol. LT - 4, pp. 1711 - 1716, 1986.

8. B. Moslehi, "Analysis of optical phase noise in fiber optic systems employing a laser source with arbitrary coherence time," *J. Lightwave Technol.*, vol. LT - 4, no.8, pp. 1334 - 1351, September 1986.
9. C.H. Henry, "Theory of the linewidth of semiconductor lasers," *IEEE J. Quantum Electron.*, vol. QE - 18, No. 2, pp. 259 - 264, February 1982.
10. A. Papoulis, "*Probability, Random Variables, and Stochastic Processes*," Mc-Graw Hill, New York, 1984.
11. A. Arie and Moshe Tur, "Phase induced intensity noise in optical interferometers excited by semiconductor lasers with non-Lorentzian line shapes," *J. Lightwave Technol.*, vol. LT - 8, pp. 1 - 6, January 1990.
12. A.Bruce Carlson, "*Communication Systems*," Mc-Graw Hill, New York, 1985.
13. S.S. Sodhi, "Effects of impairments on fiber-optic system performance," *M.S. Thesis, Virginia Polytechnic Institute and State University*, Blacksburg, Va., April 1989.
14. K. Sam Shanmugan and A.M. Breipohl, "*Random Signals : Detection, Estimation and Data Analysis*," Chapter Two, John Wiley & Sons, New York, pp. 83 - 87, 1988.
15. D. Welford and S.B. Alexander, "Magnitude and phase characteristics of frequency modulation in directly modulated GaAlAs semiconductor diode lasers," *J. Lightwave Technol.*, vol. LT - 3, no. 5, pp. 1092 - 1099, October, 1985.
16. S.C. Mettler and C.M. Miller, "*Optical Fiber Telecommunications II*," edited by S.E. Miller and I.P. Kaminow, Chapter Six (Optical Fiber Splicing), Academic Press, San Diego, CA, pp. 279, 1988.
17. D.G. Duff, F.T. Stone, and J. Wu, "Measurements of modal noise in single mode lightwave systems," *Proceedings of OFC 1985*, San Diego, CA, Paper TU01.
18. W.C. Young and D.R. Frey, "*Optical Fiber Telecommunications II*," edited by S.E. Miller and I.P. Kaminow, Chapter Seven (Fiber Connectors), Academic Press, San Diego, CA, pp.309 - 311, 1988.

19. R.E. Wagner and C.R. Sandahl, "Interference effects in optical fiber connectors," *Applied Optics*, vol. 21, No. 8, pp. 1381 - 1385, April 1982.
20. D.A. Fishman, D.G. Duff, and J.A. Nagel, "Measurements and simulation of multipath interference for 1.7 Gb / sec lightwave transmission systems using single and multi- frequency lasers," accepted for publication in *J. Lightwave Technol.*
21. M.D. Drake, "Low reflectance terminations and connections for duplex fiber optic telecommunication links," *Applied Optics*, vol. 20, no. 9, pp. 1640 - 1644, 1981.
22. A.Elrefaie, S. Tu, and M. Romeiser, "Performance degradations of 2.4 Gb/s NRZ/RZ lightwave systems due to reflection-induced phase-to-intensity noise conversion", *IEEE Photon. Tech. Lett.*, pp.173-175, July, 1989.

Vita

Ashok Srinivasa Raman was born at Tiruchirapalli, Tamil Nadu, India in the wee hours of the morning of the 7th of February, 1965. After having completed his high school education in the eastern metropolis of Calcutta, he bravely went west in search of knowledge and wisdom to the city of Bombay, where he spent four fruitful years at the Indian Institute of Technology. He graduated with a Bachelor's degree in Electrical Engineering in May, 1987. Not sure of what to do next, he took up a job with Citicorp Overseas Software Limited in Bombay and developed financial applications software for a year. At the end of that time, however, he decided to seek more knowledge and wisdom and like many bright and ambitious young men, went further west to the United States. He obtained his Master's degree in Electrical Engineering in July 1990 from Virginia Polytechnic Institute and State University. Having had his fill of knowledge for the moment (and still searching for some wisdom), he plans to work in industry for some time. He is currently single, likes to read, jog, listen to music and play soccer.

A handwritten signature in black ink, appearing to read 'Raman', with a stylized flourish at the end.